CELIAS - CHARGE, ELEMENT AND ISOTOPE ANALYSIS SYSTEM FOR SOHO

D. HOVESTADT,* M. HILCHENBACH, A. BÜRGI, B. KLECKER, P. LAEVERENZ and M. SCHOLER
Max-Planck-Institut für extraterrestrische Physik, D-85740 Garching, Germany

H. GRÜNWALDT, W. I. AXFORD, S. LIVI, E. MARSCH, B. WILKEN and H. P. WINTERHOFF
Max-Planck-Institut für Aeronomie, D-37189 Katlenburg-Lindau, Germany

F. M. IPAVICH, P. BEDINI, M. A. COPLAN, A. B. GALVIN and G. GLOECKLER
Dept. of Physics and Astronomy and IPST, University of Maryland, College Park, MD 20742, USA

P. BOCHSLER,** H. BALSIGER, J. FISCHER, J. GEISS, R. KALLENBACH and P. WURZ
Physikalisches Institut der Universität, CH-3012 Bern, Switzerland

K.-U. REICHE and F. GLIEM
Institut für Datenverarbeitungsanlagen, Technische Universität, D-38023 Braunschweig, Germany

D. L. JUDGE and H. S. OGAWA
Space Science Center, University of Southern California, Los Angeles, CA 90089, USA

K. C. HSIEH
Department of Physics, University of Arizona, Tucson, AZ 85721, USA

E. MÖBIUS and M. A. LEE
EOS, University of New Hampshire, Durham, NH 03824, USA

G. G. MANAGADZE and M. I. VERIGIN
Institute for Space Physics, Moscow, Russia

and

M. NEUGEBAUER
Jet Propulsion Laboratory, Pasadena, CA 91103, USA

Abstract. The CELIAS experiment on SOHO is designed to measure the mass, ionic charge and energy of the low and high speed solar wind, of suprathermal ions, and of low energy flare particles. Through analysis of the elemental and isotopic abundances, the ionic charge state, and the velocity distributions of ions originating in the solar atmosphere, the investigation focuses on the plasma processes on various temporal and spatial scales in the solar chromosphere, transition zone, and corona. CELIAS includes 3 mass- and charge-discriminating sensors based on the time-of-flight technique: CTOF for the elemental, charge and velocity distribution of the solar wind, MTOF for the elemental and isotopic composition of the solar wind, and STOF for the mass, charge and energy distribution of suprathermal ions. The instrument will provide detailed in situ diagnostics of the solar wind and of accelerated particles, which will complement the optical and spectroscopic investigations of the solar atmosphere on SOHO. CELIAS also contains a Solar Extreme

* Principal-Investigator
** Principal-Investigator for data phase

Solar Physics **162**: 441–481, 1995.

Ultraviolet Monitor, SEM, which continuously measures the EUV flux in a wide band of 17 – 170 nm , and a narrow band around the 30.4 nm He II line.

Key words: SOHO – Solar Wind – Solar Energetic Particles – Composition Measurements – Time-of-Flight Spectrometer

1. Introduction

The CELIAS instrument on SOHO is designed to study the composition of the solar wind (SW) and of solar and interplanetary energetic particles. It consists of three different sensors with associated electronics, which are optimized each for a particular aspect of ion composition. These aspects are the elemental, isotopic, and ionic charge composition of SW and suprathermal energetic ions emanating from the Sun. In addition, the Solar EUV Monitor (SEM) has been included into CELIAS for monitoring the absolute EUV flux from the Sun for the entire SOHO mission.

The observation of particle abundances of the solar wind and of solar energetic particles (SEP) by itself, and in close correlation with optically observable phenomena on the Sun, will allow us to tackle basic unsolved questions in solar physics. The diagnostic power of solar particle investigations for understanding heliospheric processes has been demonstrated impressively in recent years. It can be expected to advance significantly by combined in situ particle and remote optical observations possible with SOHO instrumentation. These processes include:

- feeding of the solar corona and of the solar wind with matter from the underlying solar atmosphere,
- acceleration and heating of solar wind particles in the inner corona,
- acceleration of solar energetic particles in active regions,
- establishment of the charge state of solar wind particles in the inner corona,
- processes leading to enrichments and variations in abundances (elemental, ionic charge and isotopic)

Another aspect of CELIAS is to study the composition and dynamics of interplanetary pick-up ions in correlation with the solar EUV flux. For this purpose a solar EUV flux monitor (SEM) for the wavelength range from 17 to 70 nm has been included into the CELIAS instrument as a sub-unit of the STOF sensor. The SEM serves also to monitor the total absolute EUV flux for the large EUV telescopes on SOHO.

The understanding of the phenomena outlined above requires collaboration with many other astrophysical disciplines. Among them are ground based observations including radio-astronomy data (e.g. the well known Type III kilometric radio bursts, which are related to the strong enrichment of certain species in SEPs), as well as data on the magnetic field conditions in interplanetary space. The in situ abundance results will be interpreted

in terms of solar abundances as derived from photospheric spectra, solar oscillation data from SOHO, and meteoritic composition data from various sources.

2. Scientific Objectives

2.1. Isotopic Composition of the Solar Wind

The Sun contains by far the largest reservoir of matter in the solar system. For many geochemical and cosmochemical applications it is sufficient to know the isotopic composition in some primordial meteorite classes. However, for the understanding of the early history of the solar system and for the study of its internal evolution it is necessary to know the isotopic composition of the bulk solar nebula, or equivalently, of the present-day composition of the outer convective zone of the Sun. As far as isotopes are concerned this is the least altered sample of the early solar nebula. Our understanding of elemental coronal fractionation processes allows the rather safe conclusion that, generally, the corona gives an unbiased isotopic sample of the photosphere (and, hence, the outer solar convective zone). However, isotopic compositions are only known for a very small number of elements, namely the light noble gases. It is anticipated that CELIAS will add a substantial number of elements to the list of known solar isotopic ratios.

2.2. Elemental Composition of the Solar Wind

In situ measurements of solar wind and of energetic particles on IMP, ISEE, and the most detailed ones obtained from the ULYSSES spacecraft, have shown that elements are fractionated according to their first ionization potential (FIP). Enrichment or depletion seems to be the result of a mechanism which operates in the upper chromosphere where the gas is still mostly neutral. The assumed ion-neutral separation process must be able to feed and steadily supply a fractionated gas mixture through the transition region into the corona and into the solar wind, where it becomes multiply ionized. Various models, involving gravitational settling, acceleration, and diffusion across magnetic structures in competition with the ionization process have been studied in order to explain the apparent abundance systematics. Von Steiger and Marsch (1994) have recently suggested a new mechanism in the form of a stationary diffusion process that mainly involves well understood atomic collisional physics. In order to distinguish between the different possibilities and parametrise the models, it is necessary to obtain comprehensive abundance data for some crucial elements such as C, S, and P.

From Ulysses data it has been possible to clearly differentiate between the FIP-effect operating in coronal hole associated solar wind, which produces a fractionation factor of typically two, and in low speed solar wind, the fractionation factor between low- and high-FIP elements amounts to four. From

optical observations (Widing and Feldman, 1993) it seems that abundance ratios vary considerably with the size and the activity of magnetic structures. CELIAS will be able to determine fast abundance variations on small spatial scales under all types of solar wind (and associated coronal) conditions, with an accuracy that depends, of course, sensitively on the absolute calibration of the different sensors.

CELIAS will be able to directly determine the impact of solar and coronal processes which manifest themselves in the charge state distributions of minor ions. The most prominent and simple example of remote diagnostic is the determination of the coronal temperature via the so-called "freezing-in temperature" of a given species. Because of its wide ranges in energy, mass and charge state, covering the very same ions that are emitting "cool" EUV lines in the upper chromosphere as well as "intermediate-temperature" and "hot" EUV and X-ray lines in the transition region and in the lower corona, the CELIAS instrument can provide valuable information on the atmospheric plasma state which is otherwise not accessible.

2.3. Composition and Energy Distribution of Suprathermal Particles

CELIAS will provide a means to correlate directly the solar energetic particle (SEP) observations with optical and EUV flare observations obtained on the SOHO spacecraft. Since the charge state distribution of SEPs is basically determined by the plasma conditions at the acceleration site, a detailed measurement of the individual ionic charge states can be used as a diagnostic tool for the plasma parameters in the source regions. In addition, charge state anomalies have been reported in small active events. A special class of events with large overabundance in ^{3}He, which are also significantly enhanced in heavy ions, typically show higher charge states than the SEPs during typical CME events. Another unexpected finding with the early instrumentation was the large abundance of He^+ frequently observed in low intensity solar particle events, which is not compatible with ionization temperatures of $2 - 4 \times 10^6$ K as derived from the mean charge states of heavy ions. The observation of individual charge states and their relative distribution is of vital importance for the understanding of the plasma processes involved in the enrichment and acceleration.

The STOF instrument will provide measurements of the charge state composition and energy spectra of ions accelerated in interplanetary space at either transient shocks from flares and coronal mass ejections, or the shocks bounding corotating interaction regions (CIR) in the solar wind. The ion events at transient shocks may be "diffusive" events with large spatial scales, or "shock spike" events localized near the shock. The "corotating" events propagate to the orbit of Earth from the forward and reverse shocks bounding the CIR at larger heliocentric radial distances. The source dis-

tribution of these events is still not clear. Recently, observations with the SWICS instrument on ULYSSES made the surprising discovery that the corotating events appear to originate predominantly from interstellar pick-up ions (Gloeckler et al. 1994).

Comparison of energetic ion and solar wind composition using simultaneous measurements by the three CELIAS particle sensor systems MTOF, CTOF and STOF (see below) will determine whether the source distribution of the accelerated ions is the solar wind, interstellar pickup ions, or solar energetic particles. For those ions originating from solar wind or from interstellar pickup ions, the comparison will also determine the fractionation of the various ion species by injection and acceleration mechanisms. The continuous energy range of CTOF and STOF, from solar wind energies up to 1MeV/charge, and the large ion fluxes at these energies allow detailed measurements of energy spectra and spatial gradients for many energetic ion species, which will tightly constrain theories of shock acceleration (e.g. Lee, 1983). Measurements of the spectral shape at low energies should provide information of the injection mechanisms.

2.4. Composition of Interstellar Pickup-Ions

STOF (and CTOF) will measure the interstellar pickup ions originating from the ionization of interstellar gas inside the orbit of Earth. Since only atoms with high ionization potential penetrate within Earth's orbit, STOF is expected to detect only helium and neon. However, the mass resolution, large geometrical factor, and continuous observations of CTOF and STOF will allow one to detect $^{3}He^{+}$ and $^{22}Ne^{+}$ as well as $^{4}He^{+}$ and $^{20}Ne^{+}$. These species are predominantly photoionized by solar EUV radiation. The density of pickup ions depends on the current EUV flux, which determines the ionization rate. It also depends on the integrated flux over the previous several months, which determines the variable gas density within 1AU (Moebius et al.1985). Since the EUV flux is highly variable, it must be known accurately to interpret the pickup ion temporal variations and infer interstellar abundances. The solar EUV monitor provides an accurate measure of the variable ionizing solar radiation for both helium and neon, so that the first complete analysis of the pickup ion densities and variabilities can be made. The seasonal variation (Moebius et al.1984, 1986) of the ion density along Earth's orbit provides a measure of the ion "focusing cone" due to solar gravity. The combined measurement of the cone shape and the ionizing EUV flux allows an accurate determination to be made of the velocity and temperature of both interstellar helium and neon.

2.5. Heliospheric energetic neutral atoms

Heliospheric Energetic Neutral Atoms (HSENAs) can be generated by heliospheric ions, which are neutralized by picking up electrons from atoms in

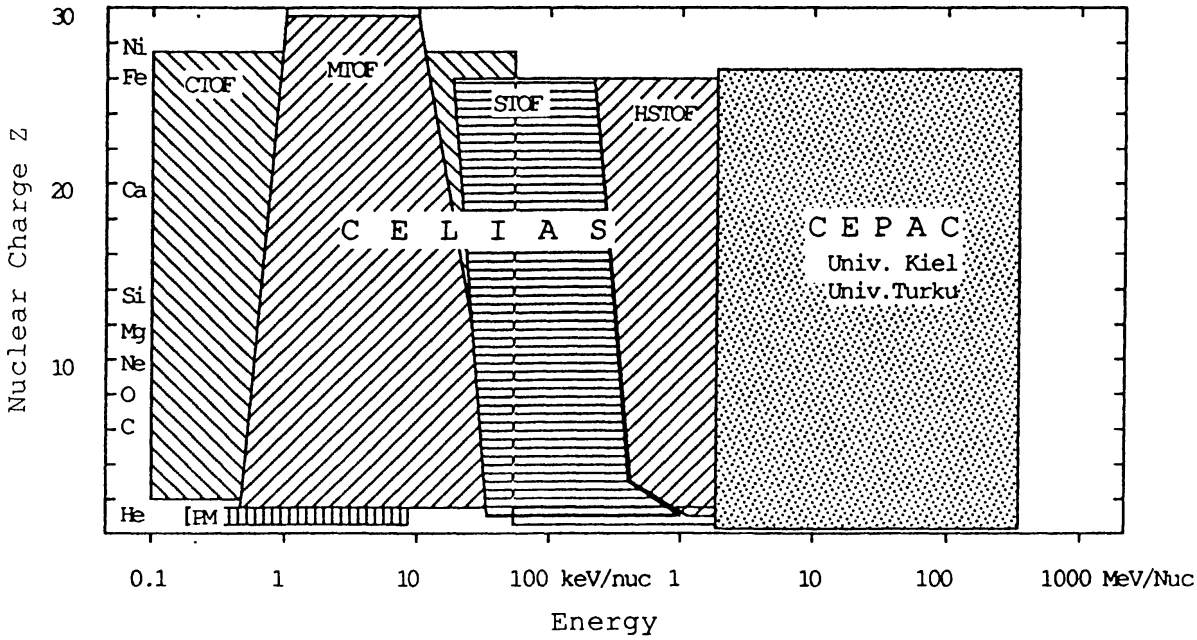

Fig. 1. Energy range of SOHO particle experiment CELIAS and CEPAC.

the ambient gas. Since the motion of neutral particles is unaffected by magnetic fields, the HSENAs trace back rectilinearly to their respective parent population. This population could be (Hsieh et al. (1992) the quiet-time interplanetary plasma, solar energetic particles (SEPs), ions accelerated in co-rotating interaction regions (CIRs), in transient shocks, and at the termination shock (anomalous cosmic rays or ACR). It can readily be expected, that most of the HSENAs, due to the energy dependence of the ion spectra and charge-exchange cross section, are of energies < 500 keV, an energy range which should be measurable by the HSTOF sensor portion of CELIAS.

3. Experiment Overview

The CELIAS instrument consists of four different sensor units: the three time-of-flight (TOF) ion sensors CTOF, MTOF, STOF, and as a piggy-back on STOF, the Solar Extreme Ultraviolet Monitor, SEM, are coupled to a common Digital Processing Unit, DPU. All three time-of-flight sensors employ electrostatic deflection systems in combination with time-of-flight (TOF) measurements of the impinging particles. In addition, the CTOF and STOF sensors employ silicon solid state detector systems to determine the residual energy, E, of the incoming particles. Thus with these two sensors the quantities energy per charge, E/Q, time-of-flight, TOF, and energy, E, are determined for the incoming particles. Now, combining energy and velocity (1/TOF) measurements yields the mass (M) of the ions, and combining energy-per-charge with velocity yields the mass-per-charge, M/Q. CTOF and STOF are aimed at different energy ranges, CTOF being devoted to

solar wind and low energy suprathermal ions, while STOF is devoted to higher energy suprathermal and low energy solar energetic particles (SEP). At the high energy end the HSTOF portion of STOF with flat deflection plates provides an E and M measurement and bridges the energy gap between STOF and the cosmic ray instruments COSTEP/ERNE (Kunow et al. 1995) on SOHO as shown in Figure 1. Thus the in situ particle instruments on SOHO, CELIAS at low energies together with the COSTEP/ERNE at higher energies, cover a very wide area in nuclear mass and energy space.

The MTOF sensor is a high resolution time-of-flight mass analyzer with a quadrupole electric field configuration. In this harmonic oscillator like electrical potential, $U \propto x^2$, the time-of-flight of ions is independent of energy or velocity and solely depends on the mass per charge, $M/Q \propto \mathrm{TOF}^2$. Because of the high mass resolution the MTOF instrument should be able not only to measure the composition of the less abundant elements in the solar wind, but also the isotopic composition of the more abundant heavy ions.

For CTOF and MTOF, wide angle ion optical systems provide the acceptance field necessary on SOHO as a stabilized spacecraft to cover the thermal width of heavy ions and to accommodate changes in the solar wind direction. Table I shows the key capabilities of the particle sensors of CELIAS.

The solar EUV monitor, SEM, is structurally connected with STOF. SEM consists basically of a Au diffraction grating in front of a set of three, absolutely calibrated, silicon light diodes, which are covered with an aluminum filter. The diodes are placed at the zero - and first order diffraction image of the Sun in order to isolate the 30.4 nm He II line, and relate it to the zero order EUV image flux of the sun.

The digital processing unit, DPU, serves all three sensors by fully handling the communications with the spacecraft. It receives rate and pulse-height data from each sensor, classifies, compresses, stores and formats it for conveying the data to the spacecraft telemetry. It also handles the experiment control through the commanding system and surveys the CELIAS housekeeping data. It also controls the sensor switching into the various operational and testing modes.

Principle of operation, details of the sensors design and its operations as well as the basic functioning of the DPU are described below.

4. CTOF - Charge Determining Time-Of-Flight Sensor

CTOF determines the mass, M, ionic charge, Q, and speed, v, of individual ions from the measurement of their time-of-flight, TOF, and energy, E_d, within a preset E/Q channel. The electrostatic entrance system accepts ions with E/Q up to 34.8 keV, which corresponds to a speed of 976 km/s for Fe^{8+}. In order to cover the entire thermal width of the solar wind distribution

TABLE I
CELIAS Experiment capabilities.

Sensor	Area/G.F.	$\Delta E/E$	Efficiency
CTOF	0.08 cm^2	0.04	0.25 - 0.65
MTOF	0.013 cm^2	0.03-5	0.03 - 0.1
PM	$7 \times 10^{-5} cm^2$	0.05	
STOF	0.1 cm^2 sr	0.1	0.02 - 0.4
HSTOF	0.1...1.2 cm^2 sr		0.02 - 0.4
Mass Resolution		M/ΔM> 100 (MTOF)	
Charge Resolution		$\Delta Q \approx 0.3 - 1$; $4 < M < 60$ (typical for CTOF and STOF)	
Energy Ranges		0.1 to 1500keV/e	

function and changes in the average direction, the entrance ion optic system roughly accepts a solid angle of 30° × 50° solid angle. This corresponds to a ratio of thermal/kinetic energy of about 0.15, e.g. $T = 2.3 \times 10^6$K, for a bulk speed of 500 km/s. In order to achieve a good time-of-flight and energy resolution of the solid state detector over the entire energy range of the instrument, the ions are post-accelerated by an acceleration voltage of up to 30 kV before they enter the TOF section, which is kept at a high voltage. The measurement of E/Q, TOF, and E_d are combined to yield the mass Mi:

$$Mi = 2(TOF/s)^2 \times \alpha_1 \times E_d$$

and the mass per charge M/Q of the ions,

$$M/Q = 2(TOF/s)^2 \times \alpha_2(E/Q_d + U_{acc})$$

where s is the TOF path length, and α_1 and α_2 are parameters which denote the energy loss in the entrance carbon foil and of the solid state detector. They are energy and species dependent and are determined in calibrations at heavy ion accelerators. Figure 2 displays a cross section and Figure 3 a photo of CTOF. The major functional submodules are indicated. All electronics on the postaccelerated potential level are situated in a "HV bubble".

4.1. The CTOF Entrance System

The CTOF Entrance System consists of a 180° hemispherical electrostatic energy analyzer situated between two quadrupole lenses. The quadrupole lenses adapt the fan-shaped field of view of the analyzer to the required

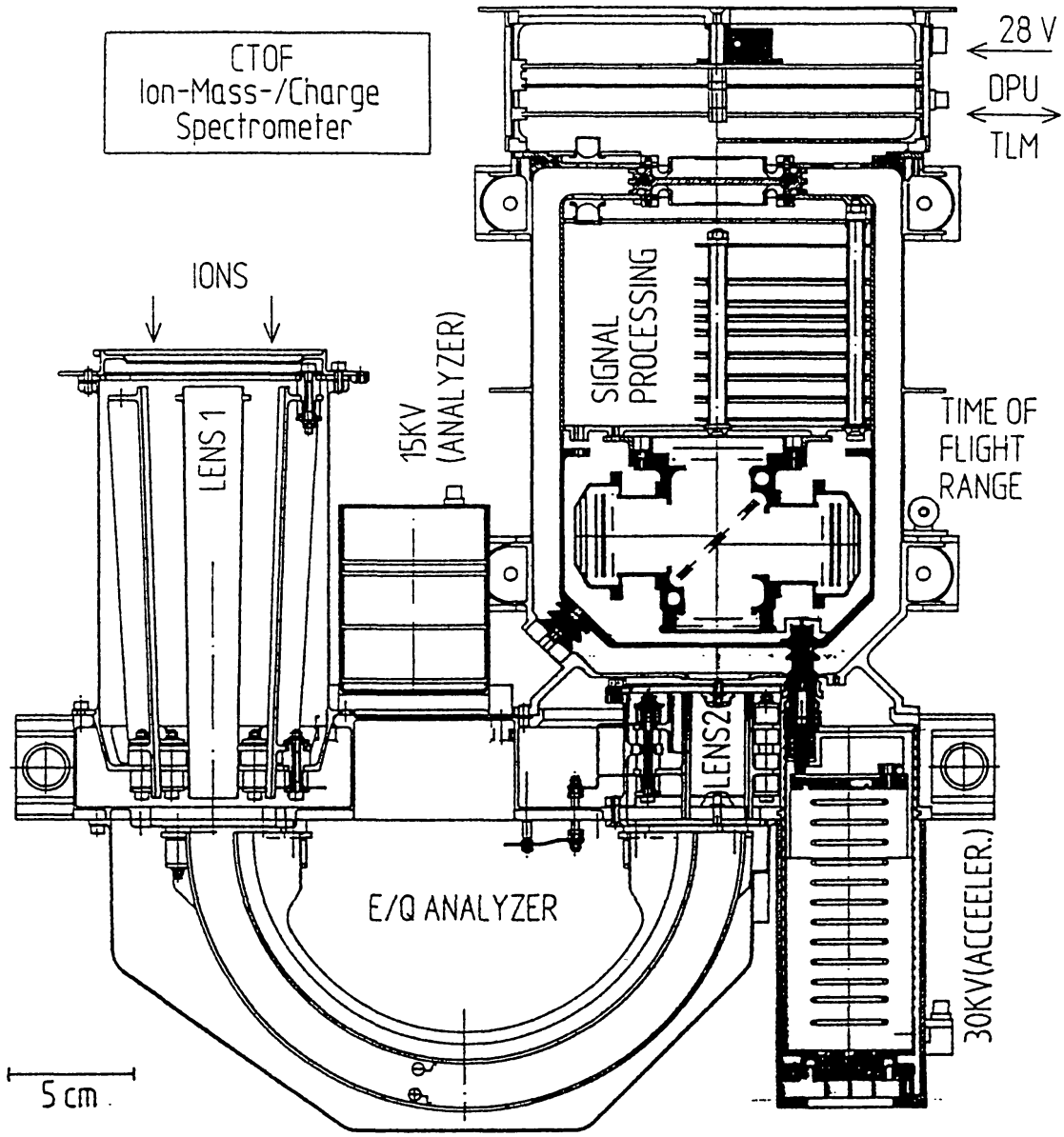

Fig. 2. Schematic cross-sectional view of the CTOF sensor.

conical one for the incoming solar wind and to the subsequent TOF system. The bandwidth in E/Q of 5.5% is a compromise between a large geometry factor and E/Q resolution. The large effective area of $\approx 0.1\text{cm}^2$ yields count rates in the order of 100/s for rare ions such as iron.

To reduce background pulses at the carbon foil generated by solar UV photons, all electrodes of the entrance system are coated with CuS that minimizes specular reflection of light. Due to the UV suppression, only 3 photoelectrons/sec are emitted for a typical flux of $2.7 \times 10^{11}\text{sec}^{-1}\,\text{cm}^{-2}$ solar Lyman-alpha.

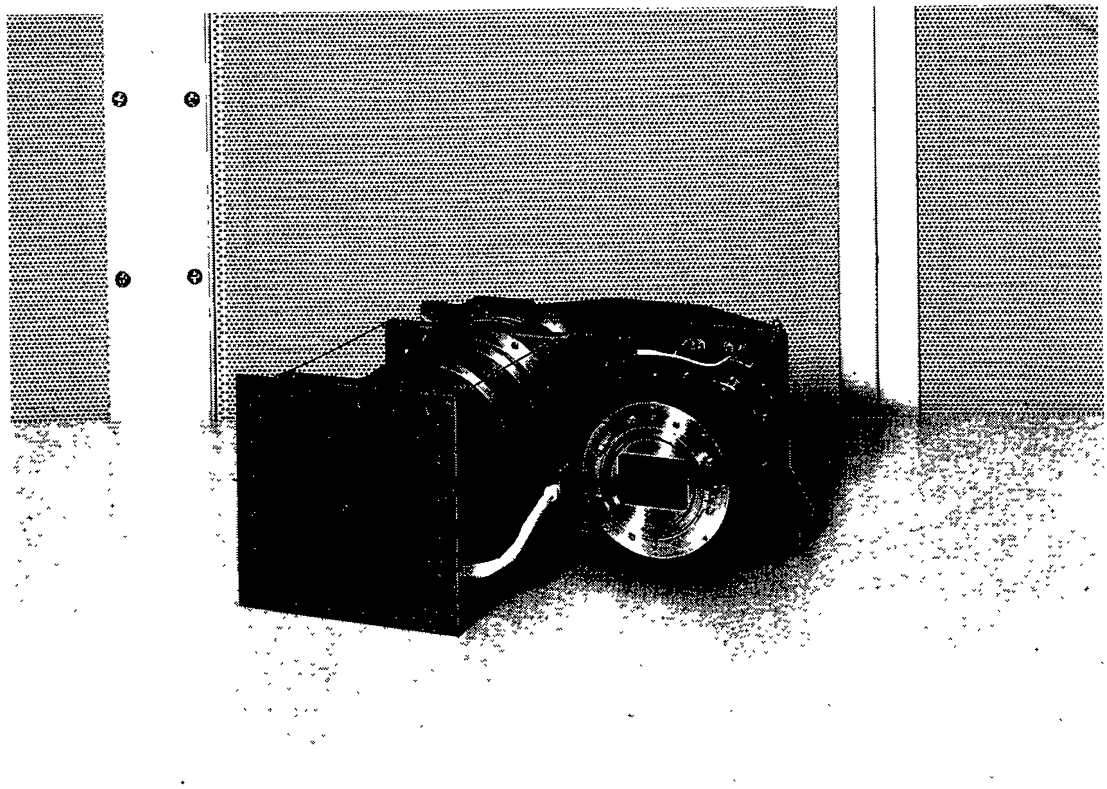

Fig. 3. The CTOF sensor.

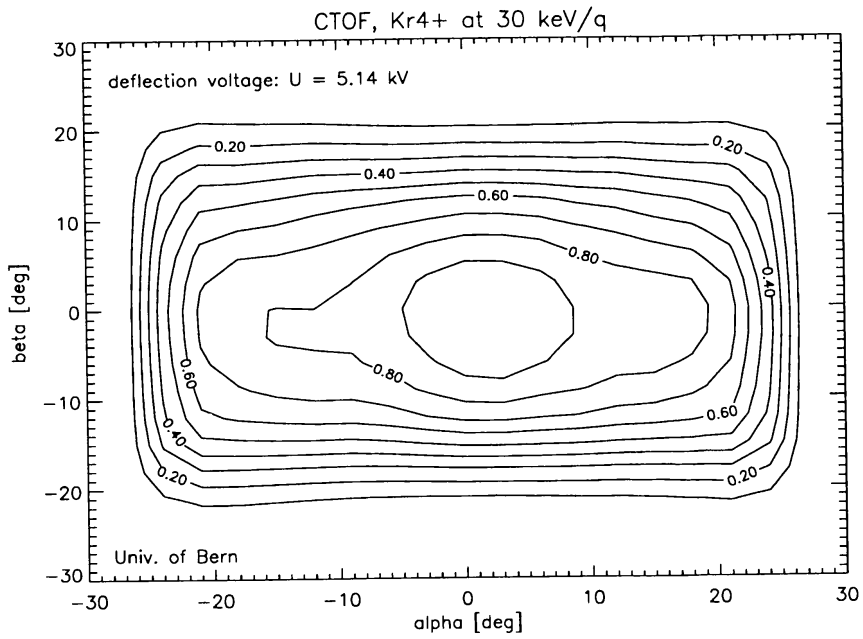

Fig. 4. Angular acceptance of the CTOF entrance system in the ecliptic plane (alpha) and perpendicular to the ecliptic plane (beta).

The measured solar wind ion distribution function is represented by differential slices in E/Q while integrated in angular space. The entire energy

TABLE II
Properties of the CTOF entrance system.

Parameter	
Effective Area	0.08 cm^2
Energy Resolution	0.055 FWHM
Angular Acceptance	±25° FWHM (ecliptic)
Angular Acceptance	±15° FWHM (perp. to ecliptic)
UV suppression	5×10^{-10}, 3 photoelectrons/s from Carbon foil

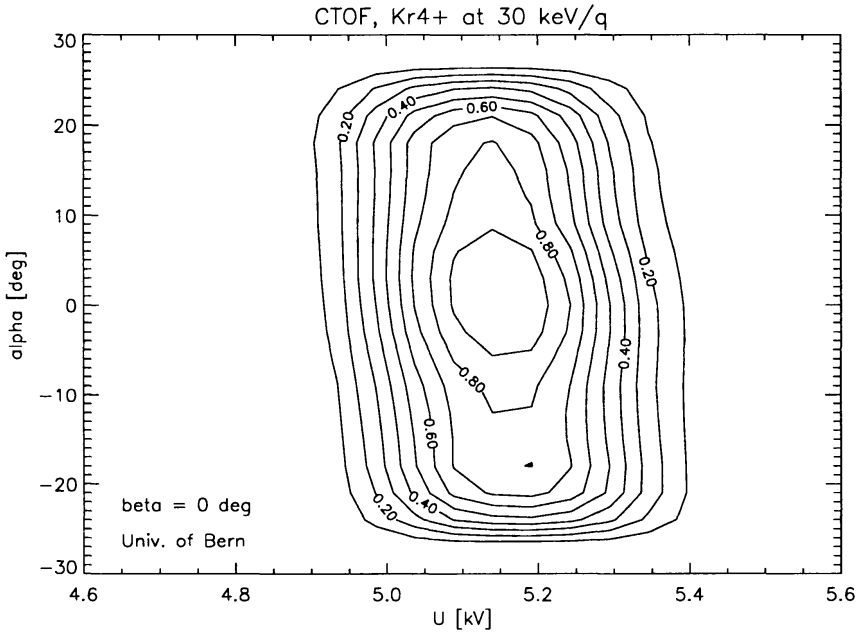

Fig. 5. E/Q resolution and angular acceptance in the ecliptic plane of the CTOF entrance system.

range of CTOF from 34.8 keV/Q down to roughly 0.3 keV/Q is covered by 117 voltage steps of 4.09% each within a full cycle of 300 sec. Due to the large effective area, the analog and digital electronics would be saturated by SW protons and helium. In order to eliminate the bulk of these ions, a fast analog identification system, the PID, can be incorporated optionally on command during the cycle.

The CTOF entrance system was calibrated at particle accelerators. Measurements of its angular response and energy resolution are shown in Figures 4 and 5, respectively. The experimental results match well the calculated linear transfer model of Oetliker (1993) for the system. The properties of the CTOF entrance system are summarized in Table II.

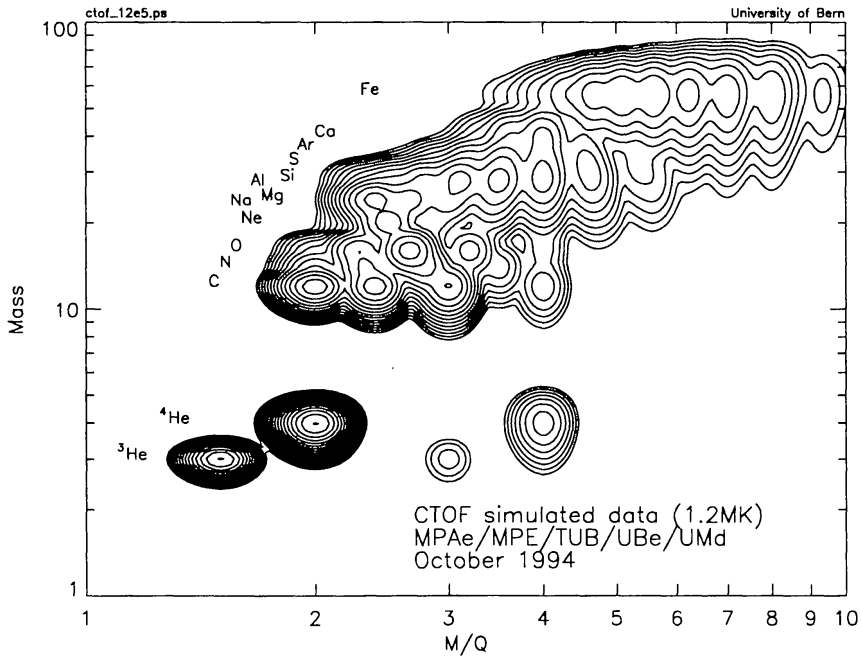

Fig. 6. Contour plot of the CTOF instrument response for a solar wind speed of 500km/s, a He/O ratio of 75, a H/He ratio of 25, and a coronal temperature of 1.2×10^6K and an integration period of 24h. Contour lines for the count rates are logarithmically spaced, starting with 1, 3, 10, .. counts.

We performed a response simulation of the CTOF sensor. For that purpose, a postacceleration voltage of 30 kV was assumed. Transmission and energy resolution of the entrance system are taken from calibrations of the flight model. The performance of the TOF section is derived from measurements of the carbon foil response by Gonin (1994), of the response of the solid state detector by Oetliker (1993), and from TOF calibrations of the flight model of the predecessor instrument SOWICOMS (flown in 1989 on the USSR PHOBOS probes, Grünwaldt et al., 1990), which employed the same geometry of the TOF section as CTOF. The assumed solar wind parameters are: speed 500km/s, coronal temperature 1.2×10^6K, and particle density 10cm^{-3}. The charge state distribution of the solar wind was taken from Arnaud and Rothenflug (1985, 1994) and mass abundances were taken from measurements of solar energetic particles by Breneman and Stone (1985) . The response function of the PID (fast analog identification system) is also included (suppression factor of 90% for $^4\text{He}^{++}$, and 100% for protons). The results are plotted in Figure 6 for an assumed integration period of 24 hours. The lowest contour line in Figure 6 represents the one count level. For comparison, the one-day integration period of CTOF corresponds to a SWICS/ULYSSES measurement of more than 100 days. This improvement is due to the higher duty cycle on the stabilized SOHO platform(no spin), larger geometric factor, and the closer position to the sun of the CTOF/SOHO instrument.

4.2. Time-of-Flight and Solid State Detector System

The postaccelerating "HV bubble" contains the TOF system and the solid state detector, SSD, at an electrical potential of up to 30 keV. The electronic START signal of the ions is derived from electrons emitted from the START carbon foil at the TOF entrance. The secondary electrons are mirrored onto a micro-channel plate system, MCP, located outside the TOF path. Similarily the STOP secondary electrons are emitted from the SSD surface and sensed in the STOP MCP system. A time-of-flight resolution of better than 1 nsec is achieved for a range from 10 to 200 nsec. The SW ions finally dissipate their residual energy in the SSD. The energy signal is then pulse-height analyzed. The SSD is an ion implanted Silicon detector with an active area of 25mm^2. Due to the large active area of the SSD the electronic threshold of the SSD has to be set below 25 keV. The post-acceleration voltage, however, adds sufficient energy to the multiply charged SW ions to overcome the threshold. For particles of energies below the SSD threshold a M/Q spectrum can still be derived from TOF and E/Q measurements. A full M and Q classification (see below), can be performed for all ions up to Ar with $Q \geq 1$, and to Fe with $Q \geq 2$.

4.3. CTOF Electronic System

For each high voltage step various total counting rates are stored in the DPU. These rates are: SR (start rate from the carbon foil), DCR (start/stop coincidence rate), SSR (rate of the SSD above the electronic threshold), TCR (triple coincidence, DCR and SSR), PJR and HeR (for protons and helium recognized by the PID). Recording the SR rate through a full voltage steps sequence yields a E/Q spectrum. Various selectable trigger conditions are controlled by the deflection voltage and decide, whether an event is accepted for the analog-digital conversion of the time-of-flight and the SSD energy, and for the subsequent M/Q and M classification in the DPU. By using the fast PID filter the stepping can be reduced to the E/Q range above the proton and helium peak to avoid overloading. This feature is important for the measurements of rare solar wind constituents.

Figure 7 shows typical time-of-flight and energy spectra obtained in calibration measurements with 300 keV He and Ar beams. The width of the TOF peak is dominated by energy straggling in the START carbon foil, while the width of the energy peak is dominated by straggling and nuclear defect within the SSD detector. The TOF and energy signal, digitized within the HV bubble, and the control commands are connected via HV optocoupler to the DPU, which performs all further processing as well as the sensor cycle control. As a specific feature the 30 kV cascade of the U_{acc} supply unit is contained within a 3 Bar SF_6 environment.

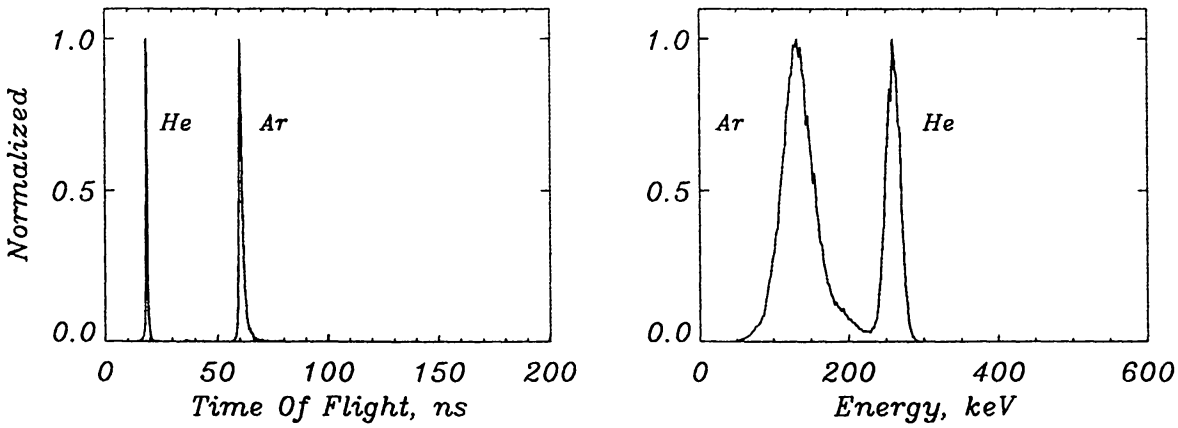

Fig. 7. Example of time-of-flight, TOF, and energy, E, spectra of He and Ar at 300 keV obtained in a calibration run.

4.4. Classification and Data Handling

The event classification system of CTOF is implemented in the DPU and serves the purpose to compress the SW data into a M/Q and M array. The DPU uses numerical approximations of

$$M/Q = f(TOF, E/Q)$$

$$M = f(TOF, E)$$

that include the parameters α_1 and α_2. The numerical expressions are represented by a total of 15 coefficients. Their default values can be replaced inflight by new values which are stored in the keep alive database within the DPU memory. The entire spectral information, processed in the DPU, is contained in: 1. Summary rate data, 2. Spectral Matrix Rates (SMR), 3. Matrix Element Rate (ME), and 4. Pulse-height data (PHA) in TOF, and E.

SMR data are stored in 508 M versus M/Q bins comprising the entire E/Q stepping range. Subsequently these bins are compressed into 21 bins by sorting in part the ion events according to a common SW bulk velocity. Details of the scheme are described in CELIAS, Experiment Operation Manual (1995). Figure 8 shows the pattern of SMR elements within the $M - M/Q$ frame. The sub-class of M/Q events without E_d signal (e.g. high M/Q at low speed events, or He^+) is stored in bins of a specific row of the matrix. The size of the cells roughly resembles the RMS width of the peaks in TOF and E with increasing accuracy towards the core part of the pattern.

For the Matrix Element Rate, ME, the SMR bin resolution is doubled in both dimensions, M and M/Q. However, in contrast to SMR, the E/Q spectral information is lost by accumulation over the E/Q scale. Finally

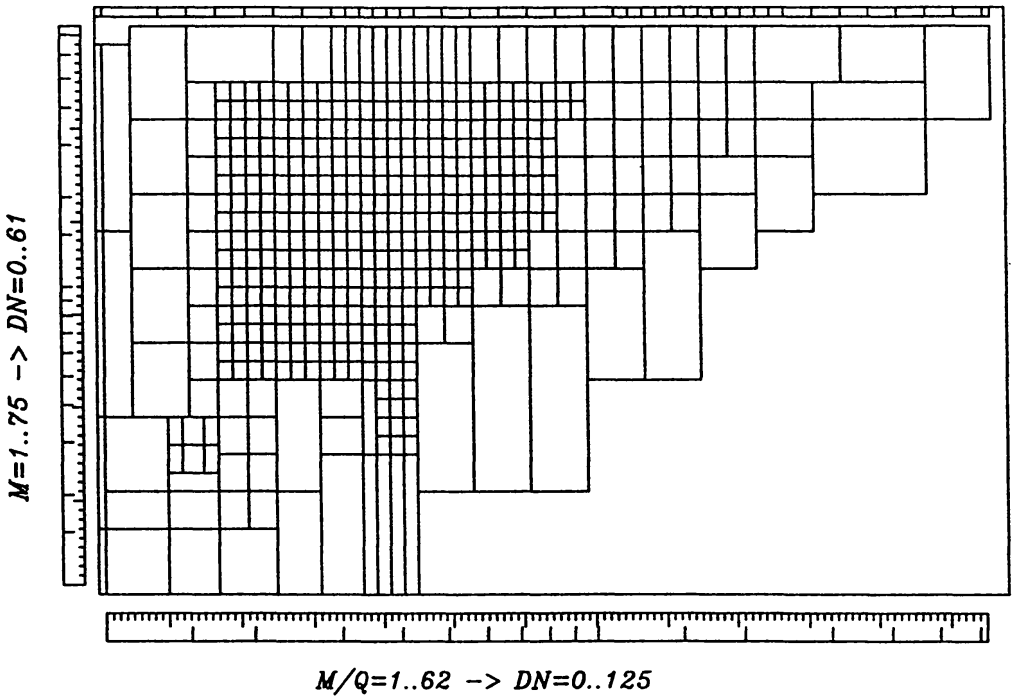

Fig. 8. CTOF SMR field definition.

up to 32 PHA events (default) are selected and transmitted to ground for each E/Q step. The PHA events are selected according to a priority scheme that can be preset by telecommand. As an option, more PHA events can be transmitted at the expense of SMR data.

5. MTOF - Mass Determining Time-of-Flight Sensor

The Mass Time-of-Flight (MTOF) sensor (illustrated photographically in Figure 9 and schematically in Figure 10) is a high mass ($\Delta M/M > 100$) resolution system that will provide unprecedented solar wind composition data over a wide range of solar wind conditions. The high sensitivity of MTOF will allow for the first time an accurate determination of the abundances of many elements and isotopes in the mass range 3 to 60 amu to be made. The velocity range of the sensor is mass dependent, extending from $\approx$200 to 1000 km/s for C and from $\approx$ 200 to 500 km/s for Fe. The MTOF sensor consists of the Wide Angle, Variable Energy/charge (WAVE) passband deflection system (described below), the time-of-flight High Mass Resolution Spectrometer (HMRS), the Proton Monitor (PM), associated high voltage power supplies, and analog and digital electronics.

5.1. The MTOF Entrance System

The MTOF entrance system is a Wide Angle Variable Energy/Charge electrostatic analyzer (WAVE). The function of the WAVE is to accept solar

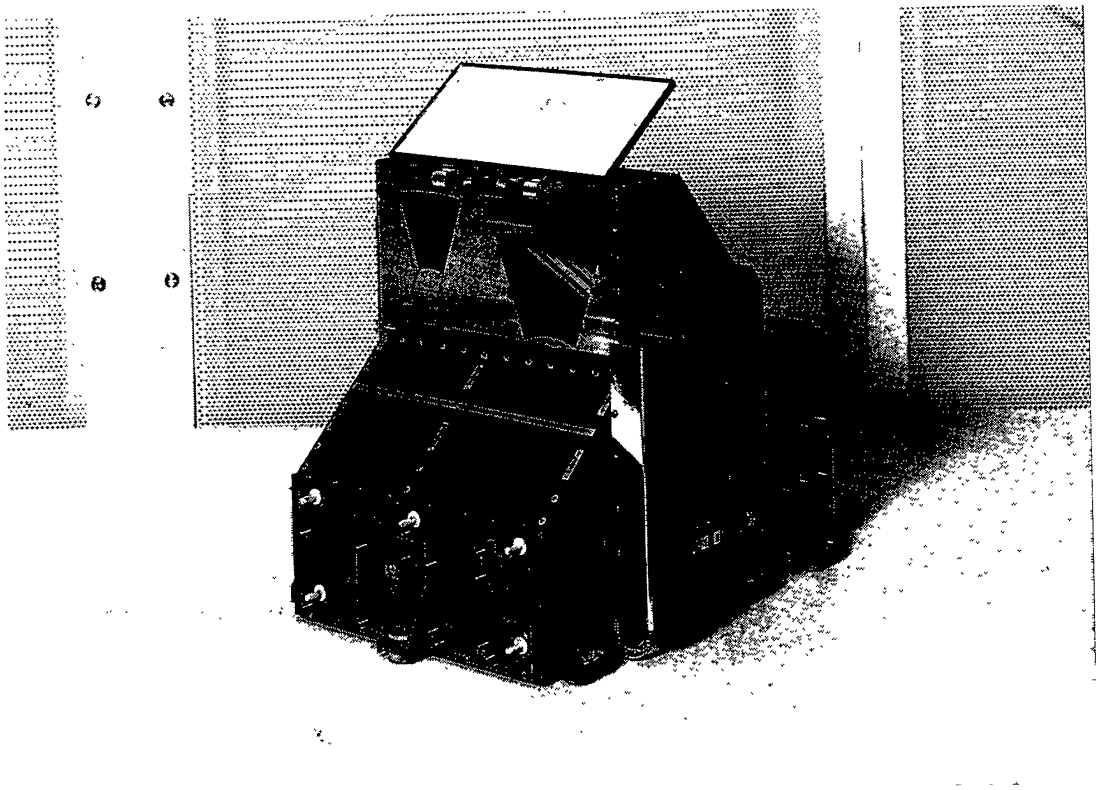

Fig. 9. The MTOF sensor.

wind ions over a large range of incident angles and ion energies and transmit them to the HMRS isochronous TOF section while eliminating the dominant proton component. In addition, the WAVE filters out incident solar UV radiation. This is especially important because the instrument points directly at the Sun during operation in the solar wind.

The WAVE consists essentially of three staggered boxes of cylindrical symmetry where a radial section is shown in Figure 11. High transparency grounded grids cover the front of each of the boxes. The voltages on the back surfaces V_{WAVE} and on three equally spaced bands along the inside perimeters are such that in each box a more or less homogeneous and constant electric field is generated.

The relative sizes of the boxes and the overall geometry are chosen such that for a given high voltage solar wind ions are accepted within an energy per charge band of a E_{max} to E_{min} ratio of about 5 and entrance angles in the ecliptic of 20° to 70°. The ideal WAVE would transmit ions as a one to one mirror system and the active area is determined by the smallest gap between box 2 and 3 which has an area of about 2 mm by 8 mm. In reality, lensing effects due to the nonideal boundary conditions of the metallized ceramics and the finite mesh size (0.25 mm by 0.5 mm) of the ground plane grids cause a divergence of the outcoming ion beam of about 10° FWHM on average for

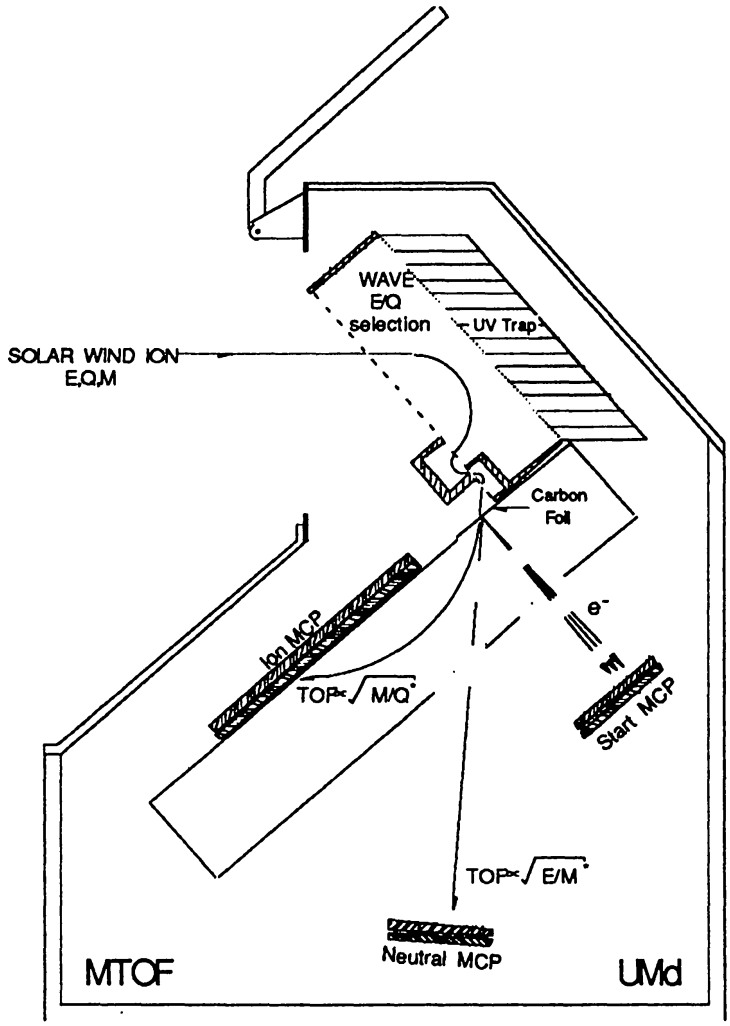

Fig. 10. Schematic view of the MTOF sensor.

different ion energies. In combination with the HMRS section, which has only a few degrees angular acceptance, this implies to some extent a reduction of the detection efficiency for a pencil beam. However, recent calibrations have shown that the effective area of the instrument meets the proposed specifications for all entrance angles. The angular acceptance of the entrance system is shown in Figure 12 and the energy response in correlation with the entrance angle in the ecliptic is shown in Figure 13. The entrance system has been tested carefully for the transmission of Lyman- alpha photons. The typical solar intensity of 2.7×10^{11}photons/sec/cm^2 Lyman-alpha photons causes the emission of about 20 photoelectrons/sec on the HMRS carbon

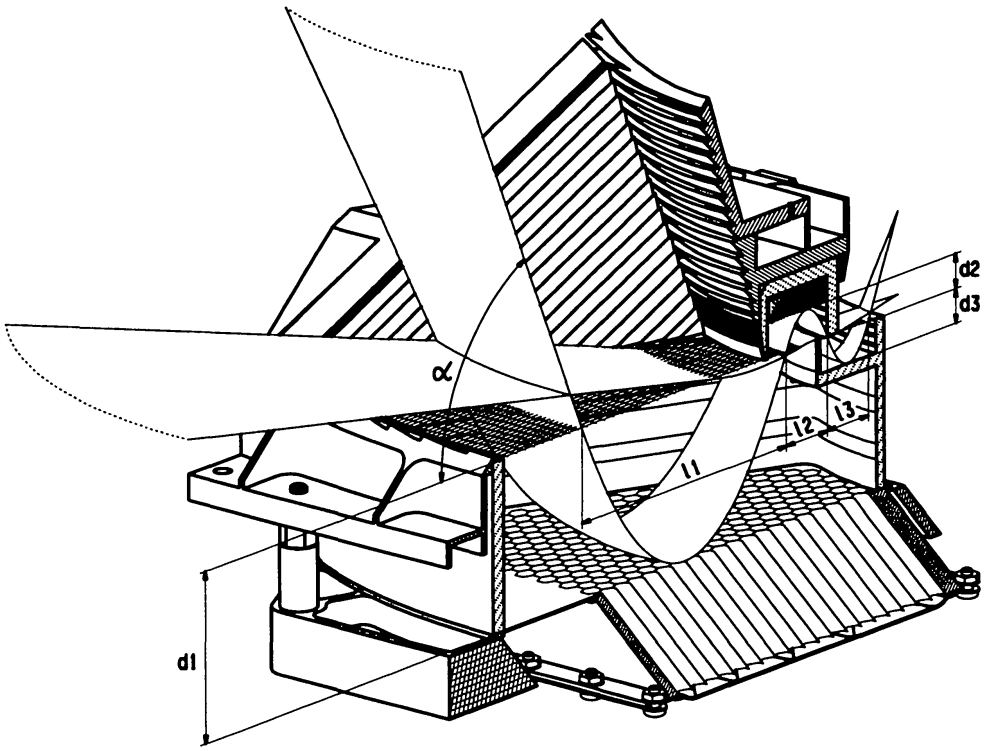

Fig. 11. Schematic view of the MTOF WAVE entrance system. α is the entrance angle in the ecliptic plane with respect to the ground plane, d_i are the box heights, l_i are the lengths of the ion path parabolas projected on the ground plane.

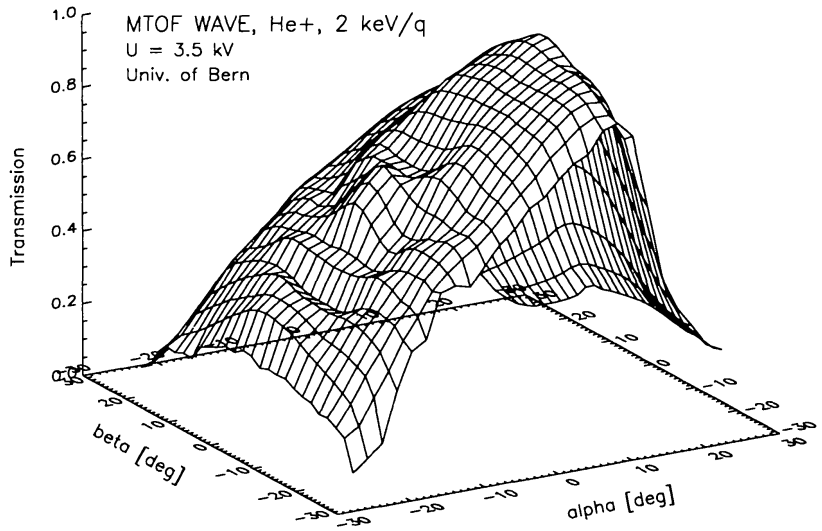

Fig. 12. Angular acceptance of the MTOF WAVE in the ecliptic plane (alpha) and the plane perpendicular to the ecliptic (beta).

foil which has an area of 4 mm by 15 mm. In Table III the typical properties of the WAVE entrance system are summarized.

TABLE III

Properties of wave entrance system.

Parameter	
Effective Area	0.1cm^2
Energy Bandpass	$E_{\max}/E_{\min} = 5$
Angular Acceptance	$\pm 15°$ FWHM (ecliptic)
Angular Acceptance	$\pm 15°$ FWHM (perp. to ecliptic plane)
UV-suppression	2×10^{-8}

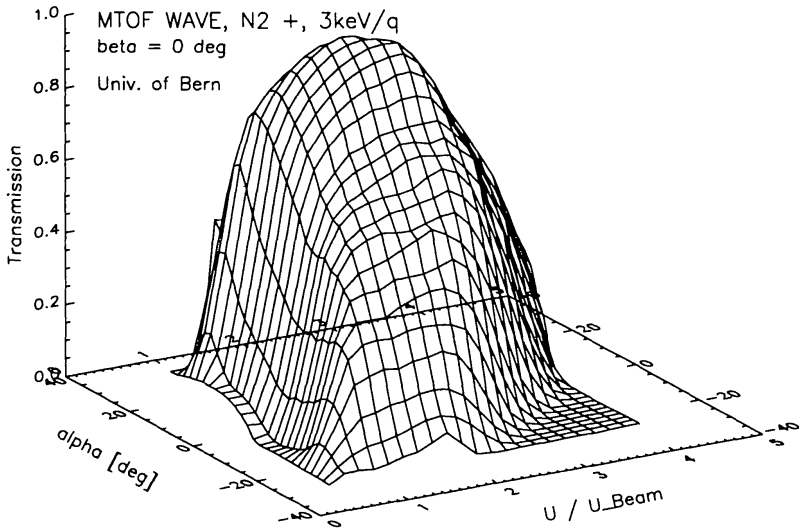

Fig. 13. Energy/Charge response in correlation with the entrance angle in the ecliptic.

5.2. The MTOF Time-of-Flight System

The heart of the MTOF sensor is the time-of-flight High Mass Resolution Spectrometer (HMRS). The principal of operation of the HMRS is based on the fact that the time of flight TOF of an ion of mass per charge $M/Q^\star$ is proportional to $(M/Q^\star)^{1/2}$ in the presence of an electric field that increases linearly with distance (harmonic oscillator). Hence, the measurement of TOF gives unambiguous values of $M/Q^\star$ for individual ions. The required electric field is produced by a combination of a hyperbolic plate set at a large positive voltage V_H (typically 25 to 30 kV) and a V shaped plate at ground potential. The high mass resolution of the MTOF sensor is due to the fact that TOF is independent of the ion energy and the angle at which the ion

enters the HMRS electric field. The value of V_H determines the maximum ion energy that can be deflected by the electric field, but does not affect the mass resolution. For solar wind ions the time-of-flight range is within 0 and 500 nsec. Since TOF can be measured with the precision of a fraction of a nanosecond, high mass resolution $M/\Delta M > 100$ is achieved. Figure 14 displays a TOF spectrum from a calibration run in which the accelerator magnet setting was varied to allow both ^{22}Ne and ^{20}Ne to alternately enter the beam. The practical implementation of the HMRS requires an accurate measurement of TOF and the conversion of multiply charged solar wind ions into singly-charged ions. This is accomplished with a combination of microchannel plate (MCP) detectors and a thin carbon foil at the entrance to the HMRS electric-field region. Ions passing through the foil undergo a large number of collisions with the carbon atoms, resulting in some energy loss, moderate scattering, and charge exchange. As a result of the charge exchange, ions with initial charge state Q emerge from the foil with charge state $Q^\star$, where $Q^\star$ is typically 0 or +1. For a precise determination of solar wind element abundances, a detailed knowledge of the final charge fractions of the different projectile species passing through the thin carbon foil is necessary (Gonin 1994). As the ions leave the foil they also produce secondary electrons that are deflected to a "Start" MCP assembly that generates a start signal for the time of flight analysis. The "STOP" signal for particles with $Q^\star > 0$ is generated at a second large area "Ion" MCP assembly located behind the ground surface of the electric field region; for particles with $Q^\star = 0$, the "STOP" signal is generated by the "Neutral" MCP. The anodes for all three MCPs provide not only the required timing signals, but also amplitude signals that are pulse height-analyzed by the electronics. These amplitude signals provide some information about particle mass and energy. In addition, the Neutral and Ion MCP anodes provide 1-dimensional position information. The Neutral position is a measure of the solar wind ion's flow direction in the solar ecliptic plane, useful for interpretation of the data. The Ion position allows us to determine the E/Q of an ion, and is also useful for rejecting background events. The entire HMRS is maintained at a 'floating' voltage, V_F, in the range -5 to +5 kV. For high solar wind speeds, a positive V_F decelerates heavy ions so that they can be deflected by the hyperbola voltage and detected by the Ion MCP. For low solar wind speeds a negative V_F will accelerate the ions before they reach the carbon foil, and thereby improve the efficiency of their detection in the HMRS.

5.3. PM - Proton Monitor

The Proton Monitor (PM) subsystem consists of a WAVE-like deflection system followed by a wedge-shaped MCP assembly that provides 2-dimensional, cylindrically symmetric, position information. The energy per charge, and hence the velocity, of incident ions is determined from the "radial" position

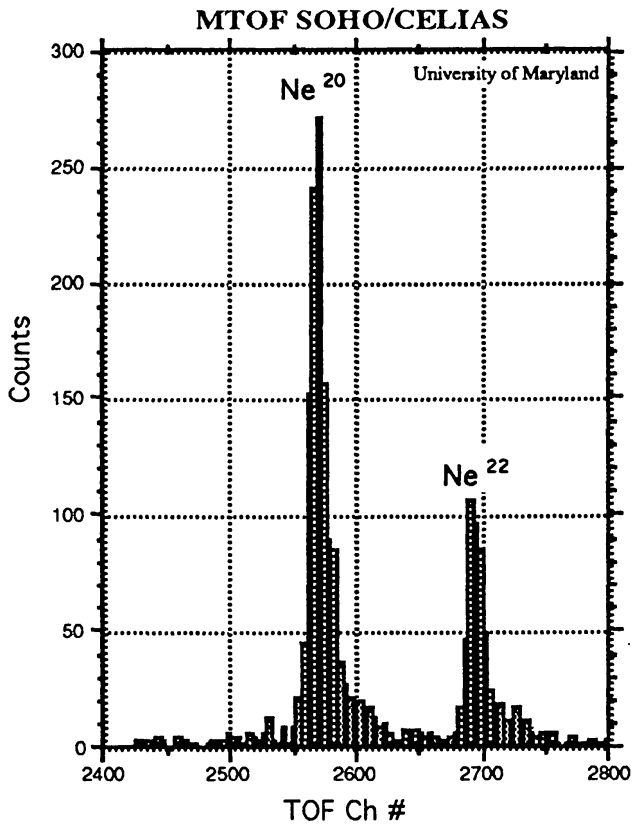

Fig. 14. MTOF time-of-flight spectrum showing the resolution of the Neon isotopes.

signal. For solar wind protons the velocity range is approximately 200 to 1200 km/s. The "theta" position signal allows one to determine the solar wind flow angle in the plane perpendicular to the solar ecliptic plane; this information will be used by MTOF and CTOF as an efficiency-factor variable. In addition, during times of low solar wind kinetic temperature, the PM measurement of O^{6+} will provide a stable in-flight calibration standard for the efficiency models of both MTOF and CTOF.

5.4. Electronics and Data System

The electronics for the MTOF instrument consist of three digital and four analog boards, which are packaged in an isolated box attached to the rear of the sensor. All circuitry dedicated to timing discrimination, internal calibrator operation, and pulse-height analysis of the Start and Stop signals are referenced to V_F, whereas the command/data interface to the DPU and the Proton Monitor circuitry are referenced to ground. The voltage difference between these two types of circuits is bridged by the use of opto-couplers. There are a total of nine power supplies incorporated in the MTOF design: one power supply for each of the MCP detector stacks; two deflection system power supplies (one for the WAVE entrance System and one for the PM); a

±5 kV acceleration/deceleration (V_F) power supply; a +30 kV power supply for the hyperbola; and the low-voltage power converter.

Most of the analysis of MTOF data will derive from the detailed PHA data. Each PHA contains the TOF, Start and Stop amplitudes, an ID to distinguish neutral from ion events, and the STOP position. A very general priority scheme is used to define three classes of events, based on upper and lower bounds (changeable by command) on the Start amplitude, Stop amplitude, Stop position, and TOF. In addition, two 1-dimensional TOF spectra are accumulated by the DPU independently of the pulse height data; these spectra are defined by ranges (also commandable) of Start amplitude, Stop amplitude and Stop position. The remainder of the MTOF data consists of the basic rates required to normalize the PHA data, singles rates for all MCPs, and both 1- and 2-dimensional rates from the PM. The MTOF data is organized as 12 steps of 5 minutes; each step will consist of a specific value for the WAVE deflection system and the V_F voltage. The PM data cycle consists of 6 steps of 5 seconds, each step corresponding to a specific value of the PM deflection system voltage.

5.5. MTOF Simulation

It is assumed that the hyperbola of the TOF system (HMRS) is at 30kV and no post acceleration/deceleration between the entrance system and the HMRS is applied. With this post acceleration voltage the performance of the HMRS mass spectrometer can be improved for certain ions at the expense of others. The transmission and the energy pass band of the entrance system are taken from calibrations of the flight model. The ionization efficiencies of particles passing through the carbon foil of HMRS are taken from calibrations at Bern (Gonin 1994). The mass resolution of the TOF section is derived from several measurements from HMRS prototypes and the flight model of MTOF.

For the simulation of the MTOF instrument response the same data set is used as for the CTOF simulation, however, the data set is enlarged by the isotopic abundances of the various elements. Thus a total of 35 different species is considered. The isotopic abundances are taken from solar system abundances given by Anders and Grevesse (1989) and from terrestrial abundance for Ca where a solar system value was not available. At nominal operations the energy pass band of the entrance system is set to transmit ions from He to Fe only. Figure 15 shows the resulting mass spectrum in the mass range from 10 to 70 amu for an integration period of 24 hours. The charge exchange of particles passing the carbon foil at the entrance of the HMRS results in mostly singly ionized species, but to a smaller extent also doubly charged ions leave the carbon foil. This effect is also included in the simulation and the respective mass peaks are indicated in Figure 15. As can be seen from Figure 15 contributions from these doubly charged ions to

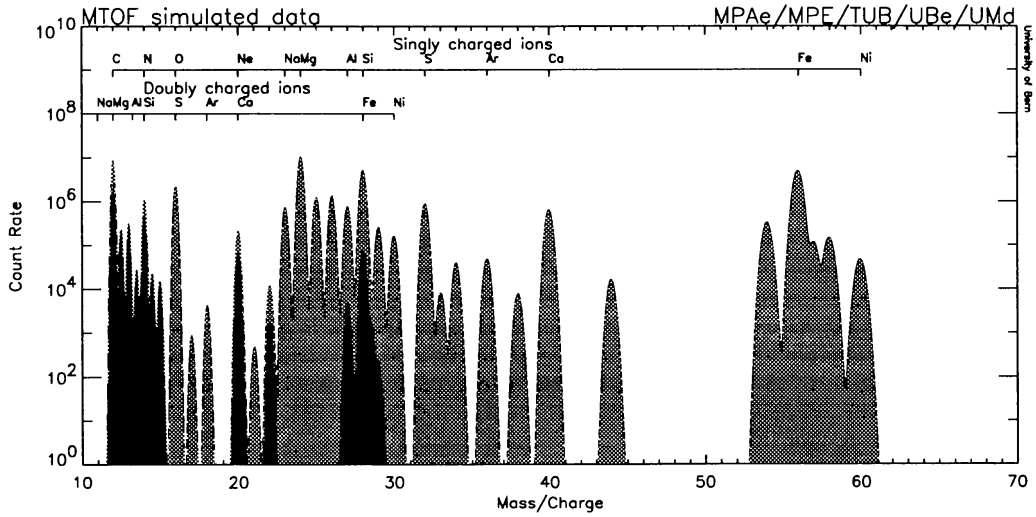

Fig. 15. Simulated mass spectrum as obtained from the MTOF sensor for solar wind speed of 300km/s and a coronal temperature of 1.2×10^6K for an integration period of 24h. Solar system abundances have been taken for all elements but Ca. The dashed curve indicates the total signal, the dark shaded areas indicate contributions from doubly charged ions.

the total signal occur mainly at the mass range from 11 to 15, and will be accounted for in the isotope evaluation using the carbon foil calibrations.

6. STOF: Suprathermal Time-of-Flight Sensor

The Suprathermal Time-Of-Flight (STOF) sensor is a particle telescope intended to measure ionic charge states of particles with suprathermal energies in the range 20 - 4000 keV/amu from just above the solar wind up to low energy flare particle energies. It thus closes the gap between the solar wind instruments (CTOF, MTOF) and the high-energy particle instruments (COSTEP/ERNE). In order to meet the scientific objectives, it has a large geometric factor of 0.1 cm^2 sr, which is achieved by a stacked multi-segment electrostatic analyzer with a large-area time-of-flight and energy measuring system. Physically, the STOF instrument consists of two separate units, the sensor and the electronic box. The STOF sensor is composed of the electrostatic deflection system, the TOF unit, the high-voltage power supplies for the E/Q-analyzer and the microchannel plates, and the digital control and analog electronics of the MCP and Solid State detectors. The STOF electronic box contains the remainder of the TOF and position measuring analog electronics, the analog-to-digital converters, and the digital event selection logic circuitry as well as the DC/DC converter. In addition, the Solar EUV Monitor (SEM) is mounted piggyback on the TOF section of the STOF sensor.

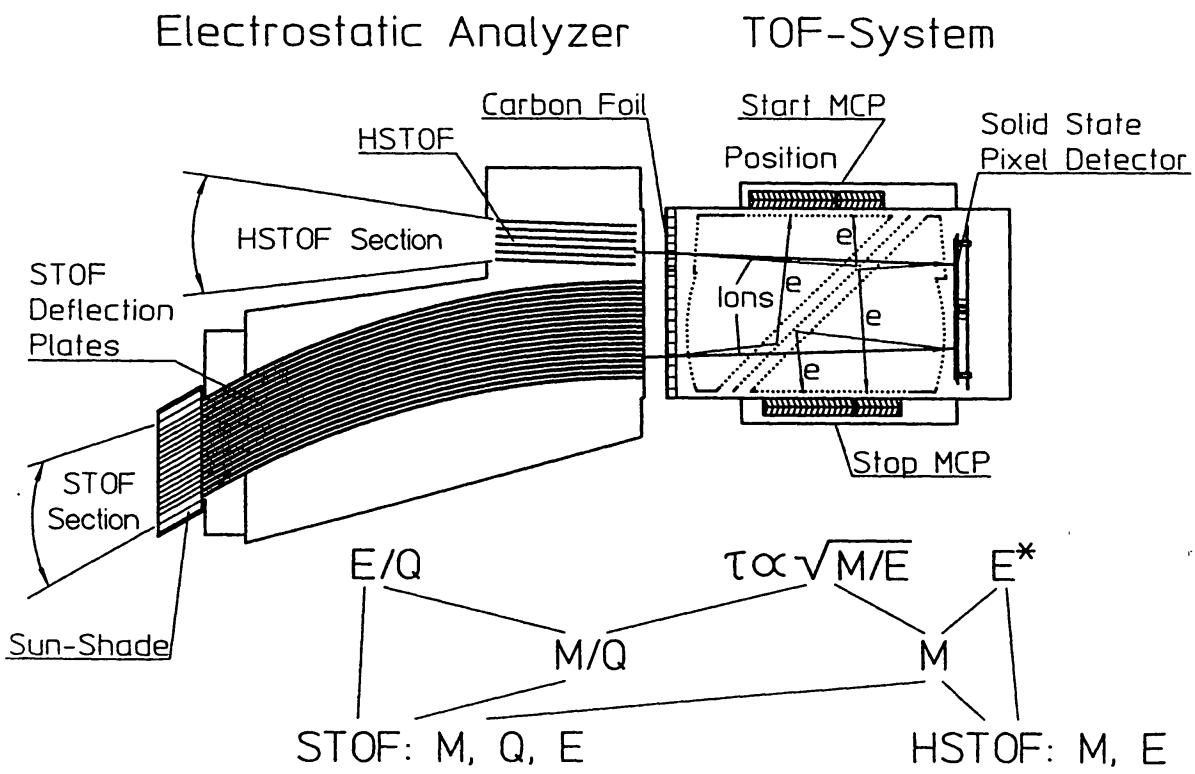

Fig. 16. STOF sensor functional cross section.

6.1. Principle of operation

Like its predecessor, the SULEICA instrument on AMPTE/IRM, and similar to CTOF, the STOF sensor combines the techniques of electrostatic analysis with time-of-flight measurement and determination of the residual energy in a solid-state detector. The energy range of 20 - 4000 keV/Q is covered by employing two sections of the electrostatic analyzer, one with curved plates (STOF main) and one with flat deflection plates (HSTOF). Incoming particles are selected according to their energy-per-charge in the electrostatic analyzer. They are then analyzed according to their time-of-flight, and finally the residual energy is measured in a solid-state detector system. Unlike in CTOF there is no post-acceleration implemented, because the suprathermal particles have sufficient energy to trigger the solid-state detector (except for the lowest energy steps). A schematic view of the sensor is shown in Figure 16 and a photograph in Figure 17.

The measurements of energy-per-charge, time-of-flight, and residual energy are then combined in the same way as in CTOF to separately determine the mass, mass-per-charge, and energy of the incoming ions. By using the position sensing of the MCPs and the position determination of the SSD-pixel-detector, the distinction between events in STOF and HSTOF can be

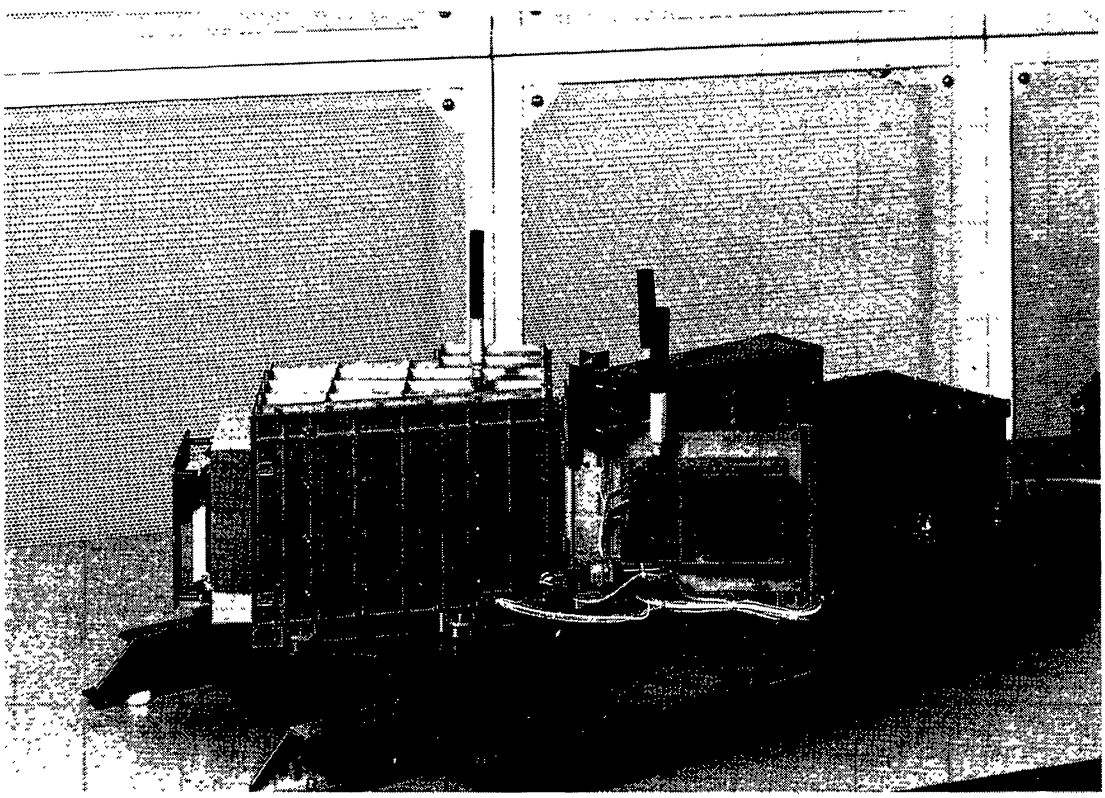

Fig. 17. The STOF sensor.

made, and also a TOF-correction can be applied for oblique flight-paths. The overall functional block diagram is shown in Figure 18.

6.2. The STOF Entrance System

The STOF entrance system consists of a stack of 18 cylindrical high-voltage plates with an entrance angle of $\pm 15°$ perpendicular to the spacecraft mounting plane. The STOF gap entrances between the 18 electrode plates are spread in their orientation by about 3°. The angular acceptance of a single gap is .5° degree. The resulting energy resolution is 10%. For realizing the 10% energy resolution the STOF deflection plates had to be manufactured with a precision of 15 microns. The radius of the STOF plates is 600 mm, the gap for the ion path varies between 3.5 and 2.8 mm and voltages up to $\pm 5kV$ can be applied to the Al-epoxy sandwich plates. Thus suprathermal interplanetary and solar ions (low-energy SEPs, Solar Energetic Particles) can be analyzed with energy per charge ratios from 20 keV/e to 1000 keV/e. The STOF entrance system has a geometric factor of about 0.1 cm^2 sr. The transmission of the entire STOF stack in energy per charge and angle in the ecliptic is shown in Figure 19. In addition to the STOF stack there is a HSTOF parallel plate stack, which gives access to the TOF system only for high energy particles above $500keV/charge$. The purpose is to measure

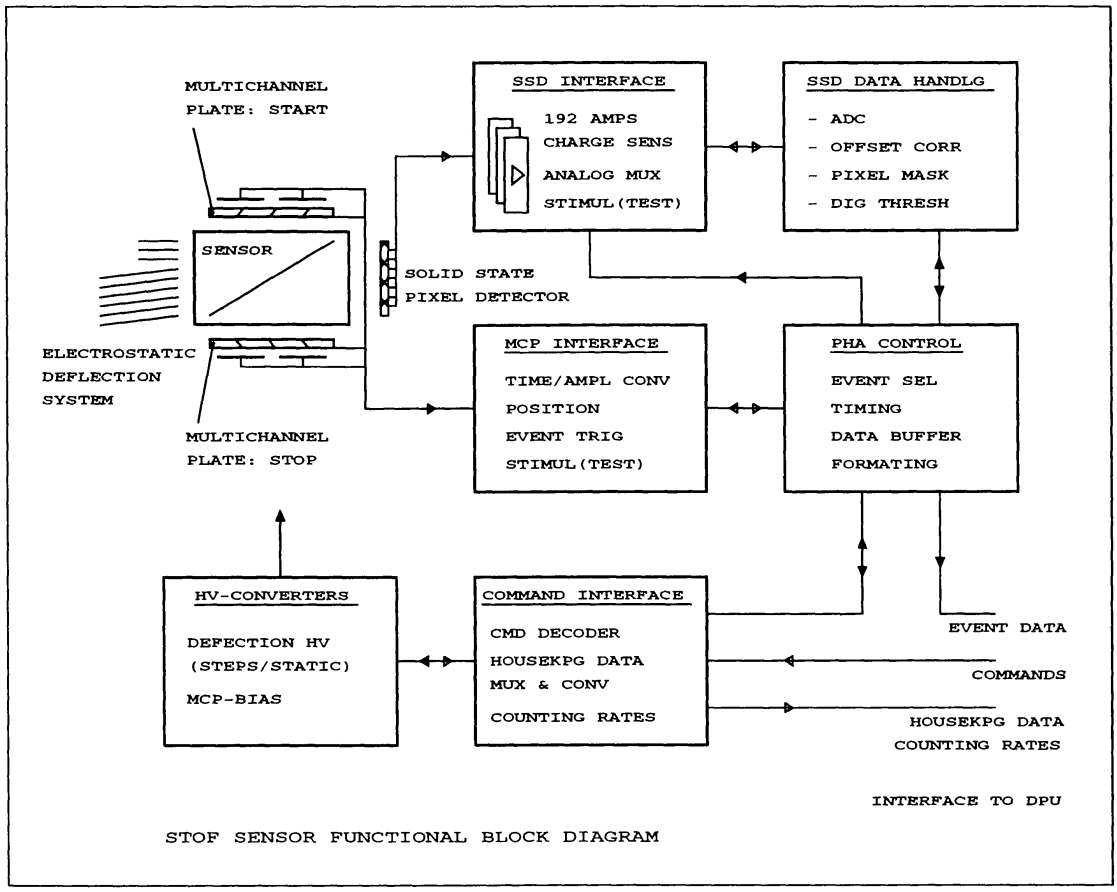

Fig. 18. Electronic block diagram of STOF.

TOF and energy of SEP particle between the STOF and CEPAC range of the SOHO instrumentation.

The aluminum electrodes of the STOF and HSTOF stacks are plated with 0.25 micrometer of gold with a rough surface. In combination with the black copper sulfide coated STOF sunshade/collimator in front of the deflection plates, the solar UV light is suppressed by at least seven orders of magnitude and the visible light by 2×10^{-6}. In the HSTOF system Lyman-alpha UV and visible stray light (zodiacal light) is suppressed by the start detection foil with a special compound coating (see below). In Table IV some properties of the STOF entrance system are summarized.

6.3. The Time-of-Flight System

The incoming ions, after passing through the electrostatic analyzer, enter into the time-of -flight (TOF) unit through a grid-supported carbon foil with a thickness of $4\mu g/cm^2$ (or in case of HSTOF a 3 layer composite Silicon-Lexan-Carbon foil, $\approx$ 28/30.5/5 nm thick, for suppression of scattered Lyman alpha) and reach the pixel solid state detector at the end of the TOF unit. The START and STOP signals are generated by secondary

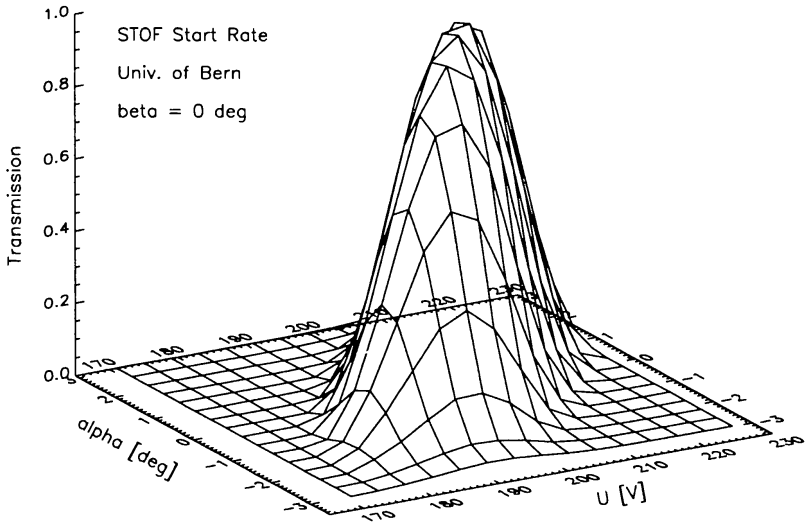

Fig. 19. Energy/Charge response in correlation with the entrance angle in the ecliptic (alpha) of the STOF entrance system.

TABLE IV

Properties of the STOF entrance system.

Parameter	
Geometric Factor	0.1cm^2 sr
Energy Resolution	0.1 FWHM
Light suppression	more than 10^{-7} for UV
Light suppression	2×10^{-6} for visible light

electrons which are emitted from the START foil and the detector front surface, respectively. These electrons are accelerated to $\approx$ 400 eV by a thin wire mesh and are then deflected by an electrostatic mirror on to the microchannel plates (MCP). The total efficiency of the TOF unit for ion detection including the geometrical effects by grids etc. varies between 30% for heavy ions such as Ne with $E > 100$ keV and 3% for protons with $E = 1$ MeV. The MCP assemblies each consist of two large 90 $\times$ 70 mm MCPs in a chevron configuration to suppress ion feedback. The voltage applied to each MCP is about 1400 V. The total MCP bias and grid voltages can be adjusted in flight via ground command up to 20% above the nominal level in order to compensate for a possible decrease of the MCP gain with time due to high counting rates during solar energetic particle events. The START and STOP

signals are processed in a 10 bit time-to-amplitude converter (TOF range: 4 to 735 nsec) and transferred to the event analysis electronics together with the front and rear MCP position flags.

6.4. The Solid - State Detector System

The solid state detector system consists of 12 detector chips mounted on six ceramic hybrids. Each hybrid carries 2 detectors and a CAMEX32 multiple amplifier chip with its associated analog and digital electronics for signal processing. The detector assembly has a total area of 105cm^2 and a SSD thickness of 300μm with an equivalent deadlayer of about 200 nm of silicon. The system is divided into 192 pixels (128 for STOF and 64 for HSTOF), each of which can be pulse-height analysed separately. The purpose of separating the large area of the detector system is (1) to reduce the effective capacity noise of the full detector area for a single pulse height event to about 8 keV (only the capacity of a single pixel of 0.5cm^2 contributes to the noise), and (2) to use the position information for the correction of the flight-path length. The output signal of each detector pixel is AC coupled via a 3.3 nF capacitor to the inputs of the 6 CAMEX32 amplifiers. The CAMEX32 amplifier chip is a specially adapted development of the Max-Planck-Institut and constitutes of 32 parallel, three-stage charge-sensitive amplifiers, which are digitally controlled and triggered for readout by the timing circuitry of the TOF section. Its outstanding linearity and the large dynamic range of $\approx$ 4000 (20 keV up to 85 MeV) is achieved by switching the feedback capacitors of the first amplification stages in two gain steps from 0.36 pF to 2 pF synchronously with the E/Q stepping of the STOF sensor.

Three corrections to the digital outputs have to be applied onboard: (1) Each of the 192 pixel amplifier inputs has a digital offset, which can be corrected to within 2 channels ($\sim$ 12 keV). (2) A masking scheme is implemented and can be activated to suppress pulse height output from pixels getting noisy during the mission. (3) The gain factor of each channel (varying up to 3%) is corrected digitally.

The TOF, the MCP position, and the solid state detector outputs, can be stimulated by a 1.2 kHz test pulse generator for in-flight calibration via ground command. The detector unit is thermally isolated from the sensor housing and is kept below +5° C by a black radiator into space.

6.5. STOF and HSTOF Control and Data Handling

The STOF fast analog electronics provide the basic counting rate information on the absolute particle fluxes while the E/Q, energy pulse height, and time of flight analysis yield detailed mass and charge information. A preselection and priority scheme is applied to cope with the high counting rates expected during solar energetic particle events. The basic STOF rates are:

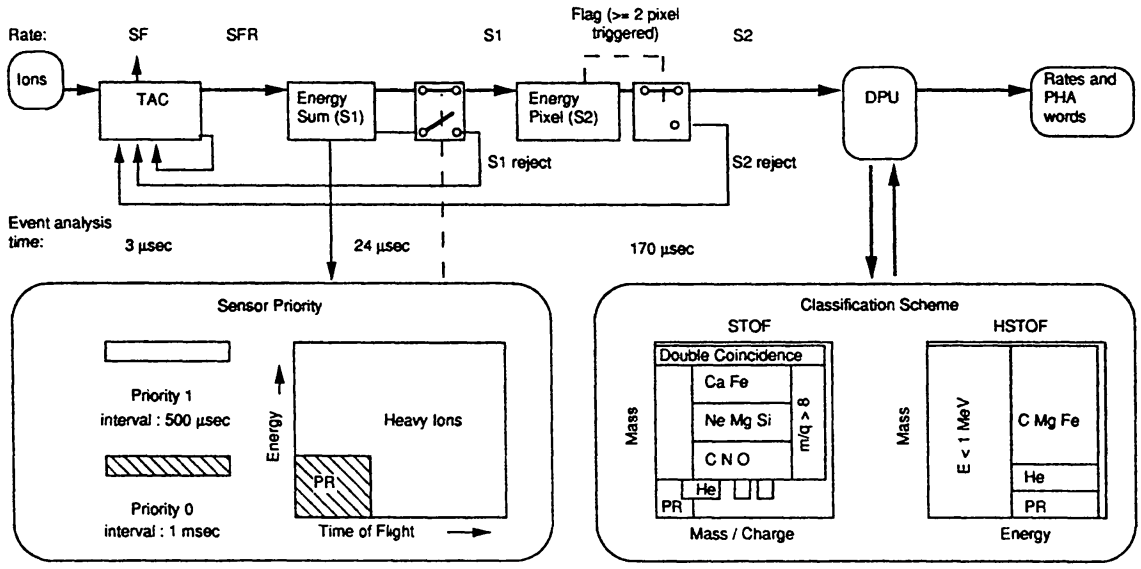

Fig. 20. STOF/HSTOF event analysis.

(1) the START MCP rate SF, (2) the TOF coincidence rate SFR (between START and STOP MCP), (3) the strobe rate S1 (triggered by TOF, E_{sum}, MCP-positions and priority flag), (4) the strobe rate S2 (for selecting the PHA words to be transferred to the DPU), and (5) the reject rates (non valid events, i.e. multiple SSD trigger, unacceptable MCP position pattern and failing priority conditions). The PHA words consist of the time of flight, the energy, the MCP and SSD positions, the gain flag of the solid state detector and the identifier for HSTOF and STOF events. The event words produced in the sensor are transferred to the digital processing unit (DPU). Then the mass and mass per charge are calculated from the TOF, the energy pulse height and the E/Q for STOF and mass and energy for HSTOF (no E/Q stepping).

In the DPU the pulse height is classified with look-up tables for fast identification and counting of ions into the M versus M/Q bins (see Figure 20). There are two different classification schemes, one for STOF and the other for HSTOF events. The set of parameters for calculating the look up tables is derived from prelaunch calibration data. The classification scheme generates 4 different kinds of data:

- matrix rates with high temporal resolution and moderate M vs. M/Q resolution (24 rates with 3.75 sec accumulation intervals (incl. priority rates);
- matrix elements with high M vs. M/Q resolution (512 elements for STOF and 240 for HSTOF) in 300 seconds accumulation intervals;
- definition of priority for PHA transfer to the telemetry;

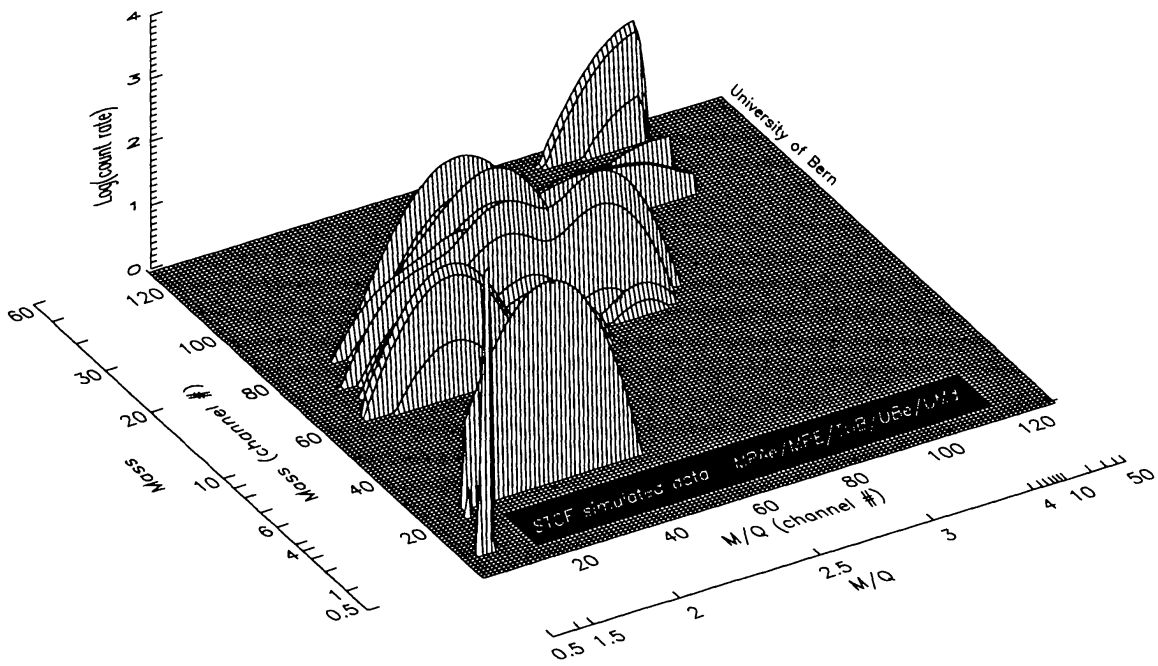

Fig. 21. Simulated instrument response for STOF sensor for a quiet period for an integration period of 24h. Details of data set are in the main text. The special data compression mechanism of STOF is also indicated, where most of the data bins are assigned to the important area in mass-mass/charge space.

– Mass and mass/charge determination.

The M vs. M/Q binning resembles the instrument resolution.

6.6. STOF and HSTOF Operational Modes

The "Nominal Mode" is the standard operational mode in orbit. The DPU controls the high voltage of the STOF electrostatic analyzer in logarithmic E/Q steps (40 steps up and 40 steps down) via command sequences sent periodically from the DPU to the sensor. A full stepping period is 300 seconds, while the various rates are binned with 3.75 sec and 15 sec resolution. The HSTOF deflection voltage is constant (set via ground command). The digital thresholds of the solid state detector and the time of flight are stepped synchronously with the E/Q deflection voltage. The gain of the solid state detector is switched in a pattern such that the gain is low in the HSTOF part while in the STOF part the gain is switched between high and low depending on the region of the STOF stepping sequence.

6.7. STOF Simulation

We performed an overall response simulation of the STOF sensor system by a Monte-Carlo calculation. The simulation included the electrostatic entrance system, the TOF and the SSD system. The transmission and the E/Q resolution of the entrance system are taken from calibrations of the flight model. The performance of the TOF section is derived from measurements of the

TABLE V
Estimated fluxes.

Source of ENH	Estimated 30-500 keV Flux $1/(\mathrm{cm}^2\ \mathrm{sr\ sec})$
ACR	9×10^{-5}
CIR	5×10^{-4}
ESP	1×10^{-2}

response of carbon foils, of silicon solid-state-detectors, and of the TOF portion of the instrument to energetic heavy ions. For STOF the same abundances of the various elements are used as for the CTOF simulation. The charge states are taken from Luhn et al., 1984. Particles with an energy of 50keV/nuc and a flux of $54 \times 10^3 (\mathrm{cm}^2\ \mathrm{sec\ sr\ MeV/nuc})^{-1}$ (Luhn et al., 1984) are considered in the simulation. This corresponds to a weak solar energetic particles event. The resulting instrument response is shown in Figure 21 for an integration period of 24h (note the nonlinear M/Q scale).

6.8. Measurement of HSENA by HSTOF

The HSTOF section of CELIAS, though not originally designed for the detection of energetic neutral atoms should be able to detect HSENA. The large geometrical factor of 1.2 cm^2 sr and the parallel-plate collimator intended to reject all ions of energies < 500 keV/e ensures that particles entering with energies < 500 keV are mainly neutral. Since the HSTOF aperture is looking at an angle 37° off the Sun-Earth line, the background generated by the sun is avoided. In addition the HSTOF TOF system is protected against interplanetary UV radiation (Lyα) by the compound entrance foil (see STOF section). The method of particle identification by time-of-flight plus residual-energy analysis further reduces unwanted background. Although the HSTOF field-of-view (FOV) is limited to $4° \times 34°$ HSTOF may capture HSENAs coming from CIRs, transient shocks, or flare events that happen to cross the FOV. As SOHO circles the Sun, HSTOF covers a belt of $\pm 17°$ of the ecliptic, which contains the apex and anti-apex of the heliosphere relative to the local interstellar medium. An estimate of the expected HSENA hydrogen fluxes from three different types of sources under the optimum condition for HSTOF is shown in Table V. The count rate of heavier neutral atoms is expected to be correspondingly lower and may be up to a few tens of counts per day.

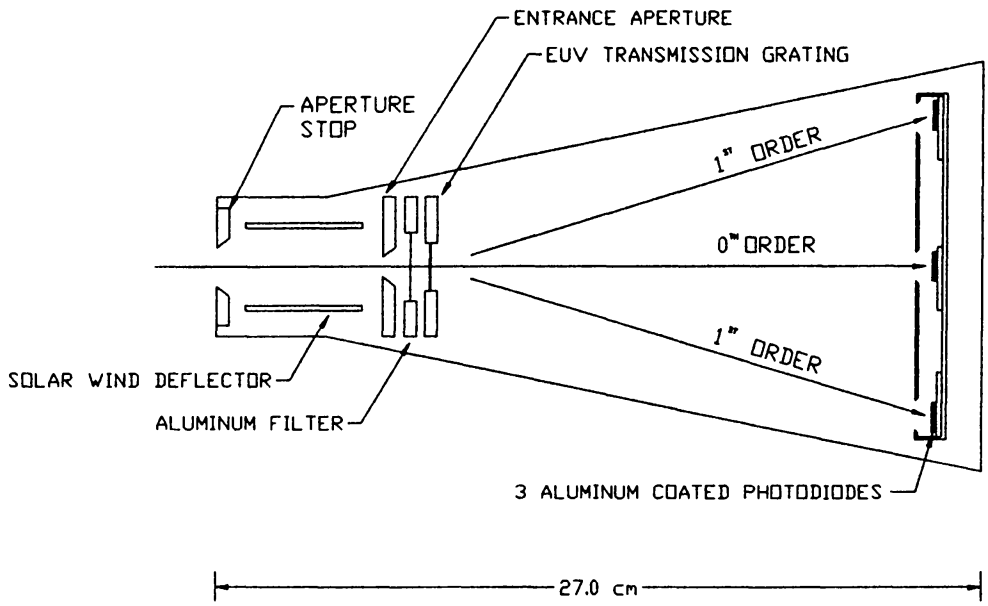

Fig. 22. Schematic view of the solar EUV monitor SEM.

7. The Solar EUV Monitor SEM

7.1. Science Objective

The Solar EUV Monitor (SEM) is a highly stable photodiode spectrometer that will continuously measure the full disk absolute solar flux at the prominent and scientifically important He II 30.4 nm line, as well as the absolute integral flux between 17 and 70 nm. These data will provide the ionization rate of the interstellar neutral helium atoms which will be observed as pick up ions by CELIAS and will provide also a reliable solar flux data base for the intercalibration of the CELIAS, CDS, SUMER, UVCS, and EIT instruments aboard SOHO.

7.2. SEM Flight Model Description and Characteristics

The SEM has been developed for inclusion into the SOHO payload as part of the CELIAS instrument and is structurally connected to STOF. The instrument is a plane diffraction grating spectrometer making use of state of the art technology in the Extreme UltraViolet (EUV). Stable and highly efficient aluminum coated silicon photodiodes detect the solar He II 30.4 nm line in the $\pm$ first order. The zero order image is measured using a similar diode and detects the integrated solar EUV in the aluminum bandpass (17 and 70 nm) which sensibly covers the helium ionization region of the solar spectrum. The incident radiation is dispersed by a high density (5000 lines/mm) free standing gold transmission grating that is placed directly behind a free standing Al filter(150 nm thick) as shown in Figure 22. Both direct and scattered light in the visible region of the solar spectrum is essentially eliminated

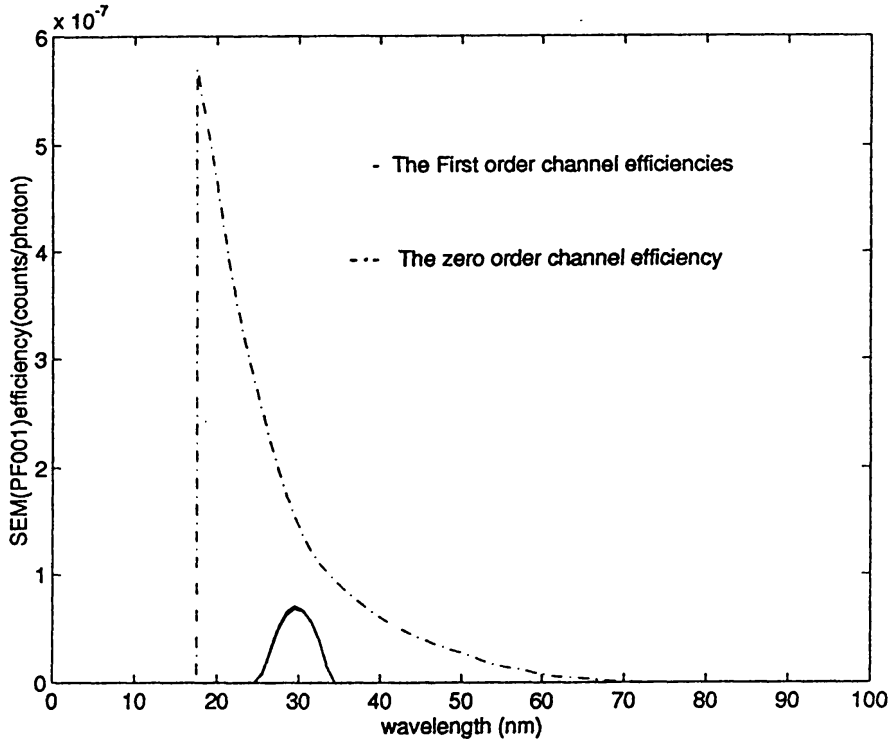

Fig. 23. Nominal response of the SEM to EUV radiation. The flight model efficiencies are still being analyzed but are higher than the above as explained in text.

by virtue of the two series aluminum metal films (i.e. the primary film in front of the grating and the aluminum film coated directly on the diode) and baffles within the optical chamber (not shown). Any potential degradation of the Al filters will be eliminated by the solar wind deflector plates in front of the entrance aperture. Due to the extended source, the sun ($\pm 1/2°$), and the finite entrance slit (2mm $\times$ 10mm) the spectrometer will have a first order bandpass of $\pm$ 4.0 nm about the helium ion 30.4 nm line as shown by the response function of the SEM pre-flight model (PF001) shown in Figure 23. A more efficient transmission grating has been incorporated in the SEM flight model (SEM001), and the National Institute of Standards and Technology (NIST) calibration data are still being processed. Preliminary results indicate that the zero order response is a factor of $\sim$4 larger and the first order response a factor of $\sim$1.5 larger than the nominal response shown in Figure 23. The diode count rate of each of the three diodes is measured by three electrometers and associated electronics placed beneath and physically isolated from the optical chamber. The diode dark current was measured by pointing the instrument directly at the sun (on the ground and on a clear day) to give a measure of the scattered light to be expected during flight. The results of this test show that the "dark current" contribution at first order is $\sim$ 0.5 pA whereas the zero order channel was 0.1 pA.

The dark current of the SEM was further calibrated against temperature and in a vacuum between - 22° and 38° C. All channels remained below 0.1

pA for temperatures below 25° C. Above this temperature channel 3 still remained below 0.1 pA while channels 1 and 2 increased by 0.1 pA at 38° C. These currents are low compared to the currents (> 100 pA at zero order and several to tens of pA at ± first order 30.4 nm) expected from the solar EUV irradiance. Absolute uncertainties (1σ) less than 10% are expected for flux determination at 30.4 nm, and less than 15% within the Al bandpass wavelength region.

8. Sensor Operational Modes

The "Nominal Mode" is the standard operational mode in orbit. The DPU controls the high voltage stepping of the electrostatic analyzer via command sequences sent periodically from the DPU to the sensors. A full stepping period is 300 seconds, while the various rates are binned with 3.75 sec and 15 sec resolution.

In addition to the "nominal" mode the sensor is able to operate in 4 different modes which are defined within the DPU program and can be controlled by ground commands. The additional modes are:

"Stand-by" - "In-Flight Calibration" - "Verifiy" - "Manual" .

The "Stand-by Mode" is the initial mode after turn ON of the instruments. All high voltages and critical parameters are set to safe levels. Only the housekeeping values such as temperatures, powerline currents and voltages are read out and transferred to the DPU. The "In-Flight Calibration" and the "Verify Mode" are used for calibration and test purposes prelaunch and during commissioning phase in flight. They send pre-programmed commands from the DPU to the sensor. The output data of these modes are used to establish the functional integrity and correct adjustment of the instruments. The "Manual Mode" allows individual setting of the sensor status by ground command, i.e. thresholds, E/Q step, solid state detector gain etc..

9. The Digital Processing Unit (DPU)

9.1. Tasks and General Structure

All three CELIAS-sensors are served by one common DPU, which is derived from the DPUs for AMPTE-CHEM, ULYSSES-SWICS and PHOBOS-SOWICOMS. Common characteristic of this DPU-family is an event driven, table-oriented, fast preprocessor for classification and priority identification. The CELIAS-DPU performs the following tasks:

1. applies pathlength correction for the time-of-flight according to the impact position (STOF);
2. calculates STOP position (X), radius (R) and angle Θ from position-sensing anodes (MTOF);

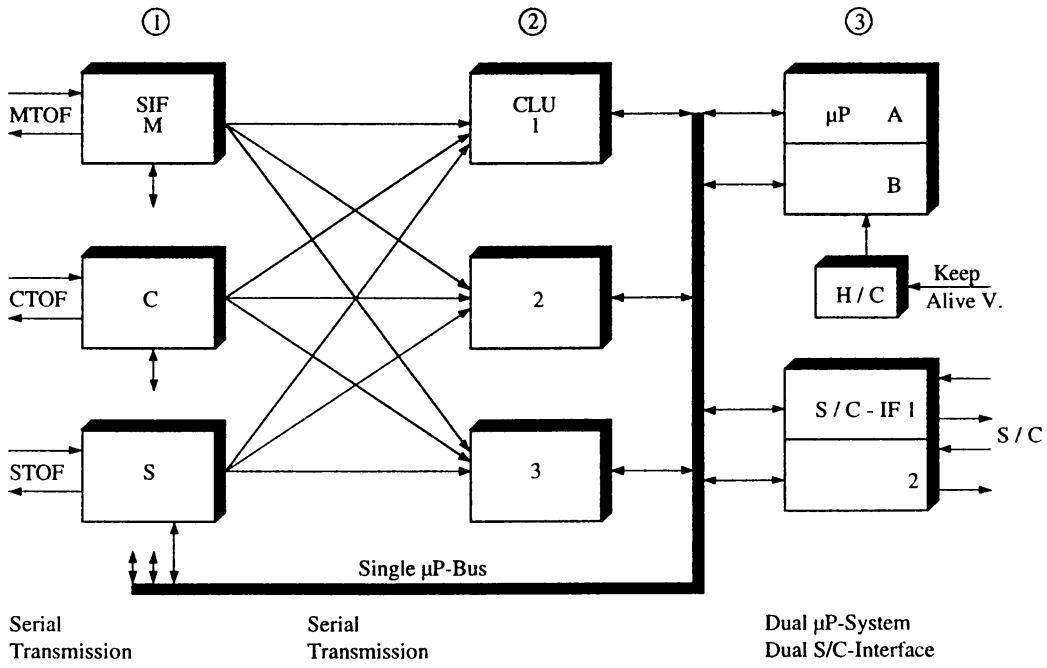

Fig. 24. Structure of the CELIAS DPU.

3. classifies events into: a two dimensional M versus M/Q matrix for each CTOF and STOF, a two dimensional R versus Θ matrix for MTOF-PM, a one dimensional M vector (MTOF) and counts them separately, with low resolution in matrix space and high resolution in time (= Matrix Rates), with high resolution in matrix space and low resolution in time (= Matrix Elements);
4. classifies events according to a priority scheme and inserts priority events into the PHA section of the Experiment Data Blocks;
5. controls stepping of the deflection voltage according to a predetermined scheme (STOF, MTOF) or an adaptive scheme (CTOF);
6. controls the sensor operational mode status and the reconfigurable DPU parts routinely or triggered by telecommand;
7. initializes the DPU program after a latch-up induced power down period;
8. monitors the housekeeping (HK) values;
9. formats and transfers the Experiment Data Block (EDB);
10. receives, decodes and executes memory load commands.

The DPU is structured into three levels (Figure 24):

1. three hardware-identical Sensor Interfaces (SIF), configurable by the microprocessor (μP)-system for a specific sensor;
2. three hardware-identical Classification Units (CLU), configurable by the μP- system for a specific sensor;
3. dual redundant microprocessor system (80C86) and dual redundant spacecraft interface.

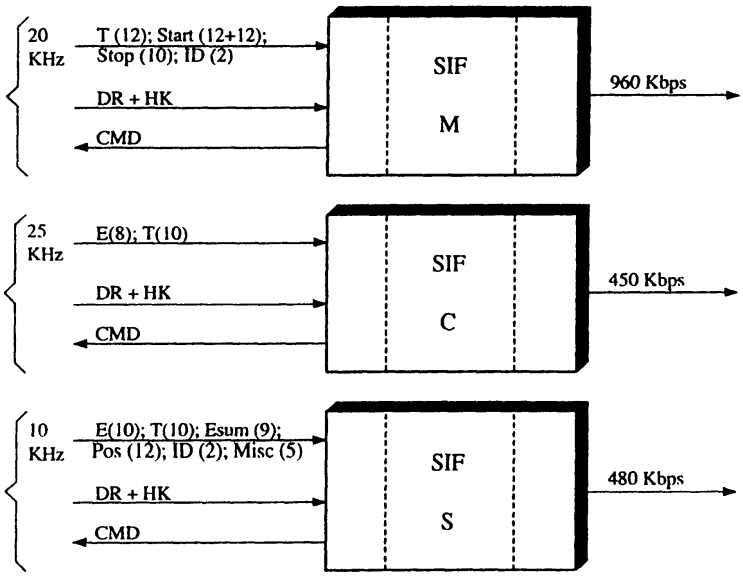

Fig. 25. Details of the SIFs.

The sequencing of the level (1) and (2) processing is event driven. The level (3) processing is sequenced by a tailored Real Time Operating System, which responds to interrupts (from the spacecraft Interface, the Classification Units, the Watch Dog Circuitry and the Latch-up Protection Circuitry) according to a priority scheme. Within level (2) each of the three CLUs can be allocated to each SIF. This switching is supported by serial data transmission from the SIFs to the CLUs. If one or even two of the CLUs should fail, the remaining ones will be shared by all three sensors according to a preprogrammed or commanded stepping scheme.The hardware of level (3) is dual redundant with the exception of the bus system. Also the DPU power converter is not redundant. The reason for partial system redundancy is that the mass for complete redundancy was not available initially. Later on the mass situation could be relieved by replacing discrete CMOS logic by ACTEL FPGAs. For schedule reasons the initial approach was retained, and the gain in mass was used for an improvement of the marginal radiation shielding.

9.2. Sensor Interfaces

Figure 25 shows the SIFs in more detail. Sensor electronics and SIFs communicate over three serial transmissions via balanced twisted pair lines. Accidental high voltage surges, entering the SIFs as common mode signal, are rejected by balloon ring coils. The SIFs comprise all the preprocessing of sensor data, which can not be handled by the uniform CLUs. The amount of these dedicated preprocessing tasks increases in the order CTOF, STOF, MTOF. The maximum event rates of 20 kHz (MTOF), 25 kHz (CTOF) and

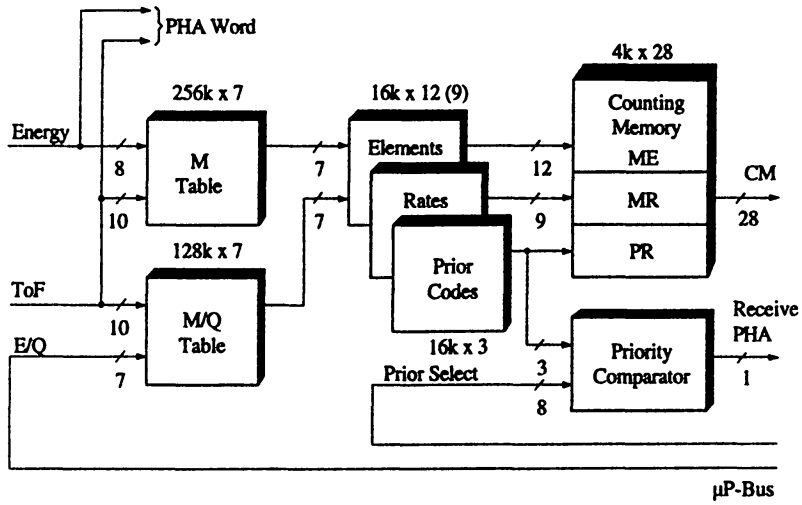

Fig. 26. CTOF classification scheme.

10 kHz (STOF) result in maximum output rates of approx. 1Mbps (SIF-M) and approx. 500 kbps (SIF-C, SIF-S), respectively.

9.3. Classification Units

In order to illustrate the classification we take CTOF as an example. Instead of the basic equations

$$M = \beta_1 TOF^2 E_{SSD}$$

$$M/Q = \beta_2 TOF^2 (\alpha_2 E/Q + U_{acc})$$

the actual sensor function is modelled by

$$\ln M = b_0 + b_1 v + b_2 u + b_3 uv + b_4 v^2 + b_5 u^3$$

$$b_0 = -3.11 \ldots\ldots b_5 = 0.0525$$

$$\ln M/Q = a_0 + a_1 u + a_2 u^4$$

$$a_0 = A_{00} + A_{01} w + A_{02} w^2$$
$$a_1 = A_{10} + A_{11} w + A_{12} w^2$$
$$a_2 = A_{20} + A_{21} w + A_{22} w^2$$

$$A_{00} = -18.330 \ldots . A_{22} = -.000077023$$

with $u = \ln(TOF/ns)$; $v = \ln(E_{SSD}/\mathrm{keV})$; $w = \ln((E/Q + U_{acc})/\mathrm{kV})$.

In case of low event rates (some events per ms) a numerical calculation can be performed by a standard microprocessor. This software (S/W)-based approach has been applied e.g. for GEOTAIL-HEP-LD. For higher event rates we use look-up tables which are calculated in a dedicated preprocessor. Figure 26 shows a straight-on implementation by a (two-stage) hardwired pipeline of fixed-sized tables. The two-dimensional table of 2^8 entries in E-direction and 2^{10} entries in time-of-flight direction delivers a seven-bit value of $M = f(E, TOF)$. Correspondingly, the two-dimensional table of 2^{10} entries in time-of-flight direction and 2^7 entries in E/Q-direction delivers a seven-bit value of M/Q. The combination of both table outputs defines one out of 2^{14} fine resolution bins within the $M - M/Q$-plane. The three Channel Address tables in the second pipeline stage compact a set of adjacent fine resolution bins to a common (Matrix Rate -/ Matrix Element -/ Prior Event -) counting channel. The E/Q entry of the M/Q-table is constant over a rather long period. It changes only with each step of the deflection voltage. Therefore, the size of the M/Q-table can be reduced to 1K7 by loading the actually valid table section with each E/Q step, provided the table is stored within a RAM.

A task specific hardwired pipeline structure supports very high event rates (some 10^6 events per s) at the expense of minimum flexibility. For medium event rates (10 ... 100 k events per s) the tables can be accessed in sequence, in case of our example in five subsequent steps. The transition from concurrent table access to sequential table access lends to a very flexible approach, characterized by a large uniform address space and by mapping of the data flow diagram into a RAM-controlled state machine, which executes the various table operations step by step. Then (1) the count of tables, (2) the table size and (3) the interconnection structure of the tables are configurable by S/W, i.e. by loading a descriptive data set into the control RAM of the state machine. Using RAMs for table storage the table contents are configurable, too. Thus the μP is capable of individualizing each CLU for each sensor. Figure 27 illustrates the inheritance of the CELIAS classification structure, which reflects the rapid progress in the capacity of the memory devices.

The uniform RAM space of the CELIAS CLUs (512K7 plus parity bit) can be configured into nine tables plus counting channels (Figure 28). Typically a table access delivers another address, which after an appropriate modification (e.g. by adding a base address) represents the pointer for the subsequent table access, or finally the pointer to the (in our example up to three) counting channels to be incremented. The contents of the tables is calculated and routinely checked (and overloaded) by the active μP. Calculation formulas and coefficients are stored in the μP-Program. These EPROM-stored coefficients can be overridden by those transmitted via the telecom-

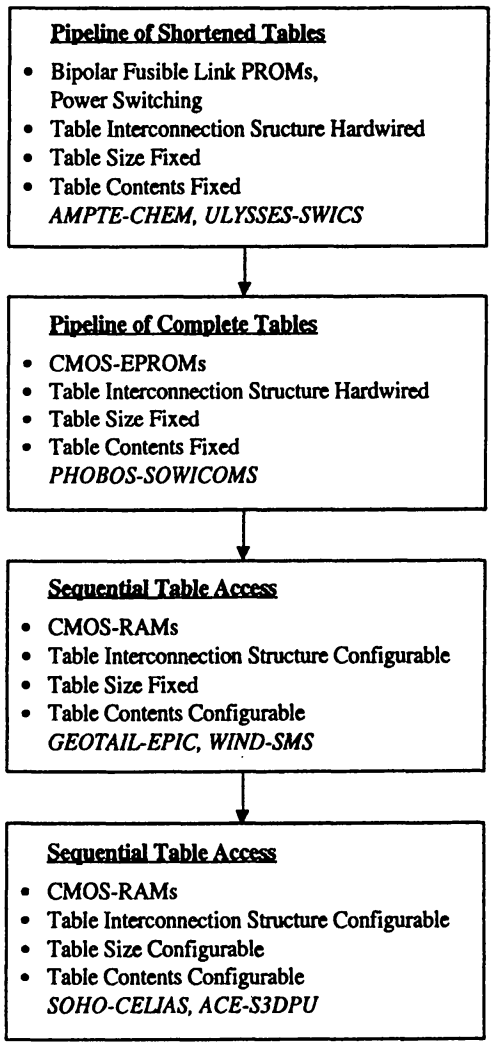

Fig. 27. Inheritance of classification structure.

mand link. Thus fine adjustements or even unexpected substantial adaptions can be applied during the mission.

In addition to the two-dimensional classification spectra, PHA-words of selected single events will be inserted into the experiment data frame. A priority Event Code is allocated to each fine resolution bin. For each event the code is compared with a μP-provided Priority Select mask. If the comparison succeeds the original event data word is read by the μP.

9.4. Protection Measures

The following protection measures are applied: (a) Cross-strapping of the CLUs. If one or even two CLU(s) should fail, the remaining CLUs will be shared by all three sensors according to a cyclic automatic reconfiguration scheme, except another configuration will be commanded. Then the EDB will be filled completely with data from the actually active sensor(s). (b) Parity Bit protection of the CLU table RAM, primarily in order to avoid

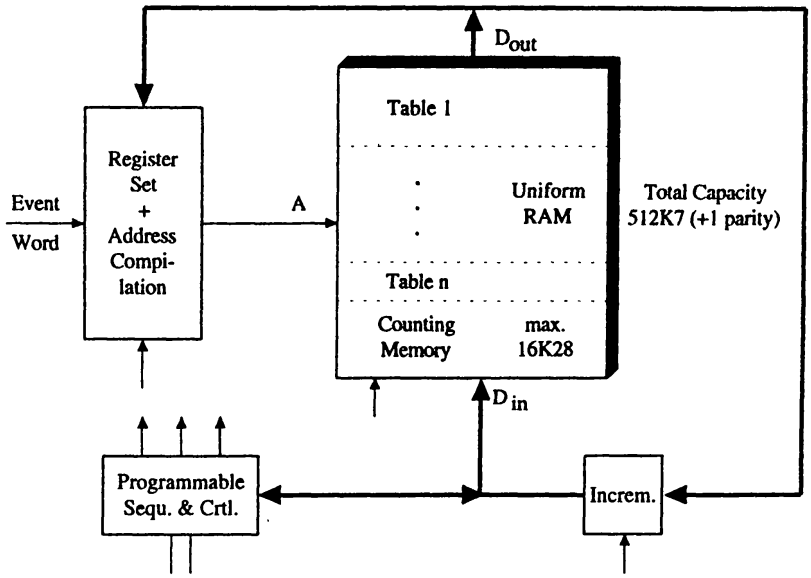

Fig. 28. Classification structure.

Single Event Upset (SEU) - induced misclassifications. (c) Refreshment of the table contents by routine recalculation from the stored parameter set. (d) Dual redundancy of the μP-system. A specific pulse command toggles a selection flipflop (minimum hard core), which locks/unlocks the μP-clock. (e) Hamming Single Error Correction (SEC) for both the processor-RAM and -EPROM. SEU-induced bitflips are corrected automatically by the SEC Coder/Decoder hardware. (f) Dual redundancy of the spacecraft-interface. Selection is done by a flipflop (powered by the keep alive voltage), which toggles with each "DPU power on". (g) Latch-up protection switches. The DPU circuitry is subdivided into eight independent supply partitions. The current into each of them is monitored. If a partition-individual threshold is exceeded, a central switch is opened and in consequence the DPU is completely deenergized (with the exception of the status memory and some status flipflops, which then are supplied by the keep alive voltage). After a short delay time the central switch will be closed (5s) and the DPU will be reinitialized, again. Since the current of the partitions varies substantially with processing activity, a single threshold would have to be set so high that a continuing subthreshold LU-current could overheat a device eventually. Therefore, two thresholds are monitored: a high threshold during regular DPU operation and a low threshold every 156 ms within a small time window (1 ms), where the DPU is driven into a sleeping state.

9.5. Packaging

The DPU is built in classic card-cage technique. A stack of nine multilayer daughterboards is interconnected by a multilayer motherboard with flexible extensions to all box connectors. The box walls are thickened to 3

mm in order to provide sufficient shielding for the high-density standard RAM/EPROM devices (tolerance dose approx. 15 krad) within the CLUs μP-systems.

Acknowledgements

The CELIAS experiment is produced in a joint effort of investigators at the following hardware-providing institutions: Max-Planck-Institut für Extraterrestrische Physik, Garching, Germany; Max-Planck-Institut für Aeronomie, Katlenburg-Lindau, Germany; Physikalisches Institut der Universität Bern, Switzerland; University of Maryland, College Park, MD, USA; Institut für Datenverarbeitung, Technische Universität Braunschweig, Germany; Space Science Center, University of Southern California, Los Angeles, USA. The authors wish to express their gratitude to all the many individuals at these institutions who have contributed to the design, fabrication, and testing of the CELIAS experiment.

The work is supported in part by DARA, Germany, under contract 50OC89056, by NASA, USA, under contract NAS-31166, by the Swiss National Science Foundation, and the PRODEX program of ESA.

References

Arnaud, M. and Rothenflug, R.: 1985, *Astron. and Astroph. Suppl. Ser.* **60**, 425

Breneman, H. H. and Stone, E. C.: 1985, *Astrophys. J.* **299**, L57

Gloeckler, G., Geiss, J., Roelof, E. C., Fisk, L. A., Ipavich, F. M., Ogilvie, K. W., Lanzerotti, L. J., von Steiger, R., and Wilken, B.: 1994, *J. Geophys. Res.* **99**, 17637

Gonin, M.: 1994, *PhD Thesis*, University of Bern, Bern, Switzerland,

Grünwaldt, H., et al.: 1990, SOWICOMS: An Instrument for Energy, Mass, and Charge Determination in Solar Wind and Mars Environment, in *Manufacturing of Scientific Space Instrumentation*, Academy of Science of the USSR, 7

Hsieh, K. C., Shih, K. L., Jokipii, J. R., and Grzedzielski, S.: 1992, *Ap. J.* **393**, 756

Lee, M. A.: 1983, *J. Geophys. Res.* **88**, 6109

Luhn, A., Hovestadt, D., Klecker, B., Scholer, M., Gloeckler, G., Ipavich, F. M., Galvin, A. B., Fan, C. Y., and Fisk, L. A.: 1985, *Proceedings ICRC* **4**, 241

Moebius, E., Hovestadt, D., Klecker, B., Scholer, M., Gloeckler, G., Ipavich, F. M.: 1984, *Nature* **318**, 426

Moebius, E.: 1986, *Adv. Space Res.* **6**, 199

Oetliker, M.: 1993, CTOF, A Solar Wind Time of Flight Mass Spectrometer with High Charge Resolution: Numerical Simulations and Calibrations, PhD thesis, University of Bern

Von Steiger, R. and Marsch, E.: 1994, *Space Sci. Rev.*, in press

Von Steiger, R. amd Geiss, J.: 1994 Composition of the solar wind, in *Cosmic Winds and the Heliosphere*, ed(s)., *Jokipii, J. R., Sonett, C. P. and Giampapa, M. S.*, University of Arizona Press, Tucson

Widing, K. G. and Feldman, U.: 1993, *Astrophys. J.* **416**, 392